TÜBİTAK

Turkish Journal of Earth Sciences

http://journals.tubitak.gov.tr/earth/

Research Article

Turkish J Earth Sci
(2021) 30: 948-972

doi:10.3906/yer-2104-16

Generation of collision-induced Early to Middle Miocene adakitic magmas in Pertek (Tunceli) area from Eastern Anatolia postsubductional setting, Turkey

Sevcan KÜRÜM[1,*], Hakan ÇOBAN[2], Pınar AYDIN[3]

[1]Department of Geology, Faculty of Engineering, University of Fırat, Elazığ, Turkey
[2]Faculty of Engineering and Architecture, University of Bitlis Eren, Bitlis, Turkey
[3]Institute of Science and Technology, University of Fırat, Elazığ, Turkey

Received: 20.04.2021 • **Accepted/Published Online:** 21.09.2021 • **Final Version:** 22.11.2021

Abstract: Early to Middle Miocene andesite-dacite porphyries are well exposed to the Pertek area of Tunceli, Eastern Anatolia, and represent an example of adakite-like magma generation in Eastern Anatolia (postsubductional) collisional setting. Mineral associations in these porphyries are composed of plagioclase (oligoclase-andesine-labradorite), amphibole (pargasite-ferropargasite), biotite, rare quartz, K-feldspar, and minor Fe-Ti oxides. Geochemically they are high-K calc-alkaline in nature and characterized by high SiO_2 (>62 wt.%), Al_2O_3 (mostly >16 wt.%), Na_2O/K_2O ratio (1.3–1.7), and Sr (generally >400 ppm) contents. Volcanic rocks display depletion in HFSEs, Nb, Ta, and Ti, and slight negative Eu anomaly; have low HREEs, Y (<11 ppm) and Yb (<0.75 ppm) contents, and are enriched in LREE, LILE, Zr, and Hf. These geochemical traits point to the adakite-like affinity for Pertek andesite-dacite porphyries, however, they present some geochemical characteristics of both oceanic slab-derived and continental crust-derived adakites and show a dual character. Enrichment in K_2O, Th, Rb, and Hf in these adakitic porphyries is mostly associated with the crust-derived terrigenous sediments during active subduction, before the Early Miocene. It is concluded that the continent-continent collision between the Arabian Plate and Eurasian Plate, break-off of Bitlis slab, and the onset of volcanism in the region was developed at Early to Middle Miocene, and the Pertek adakitic volcanism was triggered by collision- and slab break-off-induced asthenospheric mantle flows. Accordingly, our results show that a mixture of varying amounts of melts fed by sources from both amphibolitic lower crust, and subcontinental lithospheric mantle metasomatized by sediment fluids is the most likely parental magma to the Pertek adakitic porphyries.

Key words: Adakitic porphyries, hybrid source, continental collision, slab break-off, mantle flow, Pertek-Tunceli-Elazığ, Eastern Anatolia

1. Introduction

Adakites were originally defined as intermediate-acidic felsic magmatic rocks of high-silica, Sr/Y, and La/Yb originated from partially melted subducted slabs of basaltic oceanic crust (Defant and Drummond, 1990; Castillo, 2012). Although it was commonly believed that adakites originated from the subducted young (<25 Ma), and hence hot oceanic plates along the convergent margins, in recent studies some adakitic or adakite-like rocks carrying the geochemical characteristics of original adakites are documented that are not related to any slab melting or subduction zone at all (Yumul et al., 1999; Wang et al., 2005; Macpherson et al., 2006). Different models have been suggested, yet the origin and evolution of adakites or adakitic rocks are still under discussion. For example, high or low pressure fractional crystallization of (hydrated) basaltic magma and crustal contamination (Castillo, 2006; Macpherson et al., 2006); partial melting of metasomatized mantle (Guo et al., 2009; Kadıoğlu and Dilek, 2010; Şen and Şen, 2013; Çoban et al., 2020); mixing of lower crust and slab-derived melts (Çimen, 2020); FC and/or differantiation of arc-related magmas along mantle-crust boundary (Eyüboğlu et al., 2011a); partial melting of subducted young and hot oceanic crust (Defand and Drummond, 1990; Kay et al., 1993; Yılmaz-Şahin et al., 2012; Li et al., 2016); partial melting of pristine or juvenile mafic lower crust (Rollinson and Tarney, 2005; Wang et al., 2005; Castillo, 2006; Liu et al., 2008; Xu et al., 2008; Karslı et al., 2019; 2020); partial melting of thickened or delaminated continental crust (Zhang et al., 2001; Chung et al., 2003; Wang, et al., 2005; Karslı et al., 2010); slab window-related magmas along a subduction zone (Eyüboğlu et al., 2011a, 2011b; 2012), or according to isotopic signatures, those of typical subducting slab-derived adakites (O-type) with high positive $\varepsilon_{Nd}(t)$ and from postcollisional K-rich adakites (continental, C-type) with negative $\varepsilon_{Nd}(t)$ (Azizi et al., 2019) are some of the suggested models envisaged for the origin and evolution of syn- or postcollisional adakitic porphyries.

* Correspondence: skurum@firat.edu.tr

In this regard, adakite-like signature of Cenozoic intermediate-acidic porphyries from the Anatolian postsubductional tectonic settings have been reported by several workers (e.g., Varol et al., 2007; Karslı et al., 2009, 2010, 2011, 2013; Topuz et al., 2011; Eyüboğlu et al., 2011c, 2012; Şen and Şen, 2013; Lechmann et al., 2018; Yücel, 2018; Çoban et al., 2020). Some of the proposed models for their origin include: (i) pristine or juvenile mafic lower crustal melts (Yılmaz et al., 2007; Karslı et al., 2010, 2011; Topuz et al., 2011; Eyüboğlu et al., 2012; Karslı et al., 2019), (ii) lithospheric mantle melts metasomatized by slab-derived components (Eyüboğlu et al., 2011c; Lechmannn et al., 2018; Yücel 2018; Çoban et al., 2020), (iii) interaction between lithospheric mantle melts and lower crustal melts (Varol et al., 2007; Karslı et al., 2009, 2013; Ekici, 2016), or mixing of slab-derived and lower crust-derived melts (Çimen, 2020). There are, however, no simple geochemical criteria distinguishing the crustal origin from the mixed or metasomatized mantle-derived origin of the adakitic rocks.

Recent petrological and geophysical studies (e.g., Çoban, 2007; Keskin, 2003; 2005; Barazangi et al., 2006; Okay et al., 2010; Skobeltsyn et al., 2014; Karaoğlu et al., 2017, 2020; Di Giuseppe et al., 2017, 2021; McNab et al., 2018; Kaban et al., 2018; Portner et al., 2018; Agostini et al., 2019; Lin et al., 2020; Azizi et al., 2021) signify that there is a geodynamic linkage amongst the closure of the Neo-Tethys, collision of Arabia with Eurasia, break-off of the Bitlis slab, and associated asthenospheric mantle flows and uplift as major driving forces for the onset of postsubduction volcanism in Eastern Anatolia collision-related tectonic setting. Accordingly, three controversial models have been proposed for the tectonic setting of the Early to Middle Miocene magmatism in Eastern Anatolia: (i) active subduction model (Di Giuseppe et al., 2017, 2021; Agostini et al., 2019), (ii) continental extension model (postcollisional) (Topuz et al., 2019; Azizi et al., 2021) and collision-related (syn-collisional) model (Ekici, 2016). In this regard, here, we aim to study the origin of Early-Middle Miocene (16.3–15.5 Ma, Di Guiseppe et al., 2017) calc-alkaline andesite and dacite domes with adakite-like signature, cropping out in Pertek area in and along the southern side of the Keban Dam Lake area, to the north of Elazığ, in Eastern Anatolian collision zone (Figure 1), mainly discusses the role of metasomatic agents related to earlier subduction processes, and their interaction with the surrounding mantle wedge in the Early to Middle Miocene geodynamic setting of the region.

2. Magmatic activities in the southwest of the Eastern Anatolia collisional setting

The Neo-Tectonic period initiated in Turkey following the northward subduction and destruction of Neo-Tethyan oceanic crust in the Oligocene and collision of Arabian and Anatolian Plates (Şengör and Yılmaz, 1981; Koshnaw et al., 2017). Because the compression resulted from the collision of two plates, the Eastern Anatolia region had been shortened and thickened (Şengör et al., 2003; Aktağ et al., 2019) and the collision-related first Cenozoic volcanic activity was commenced with Late Oligocene-Early Miocene felsic volcanism reported from the Malatya region (Yılmaz et al., 2007) (Figure 2). Yılmaz et al. (2007) proposed that the first stage (Late Oligocene-Early Miocene) of volcanism was formed by anatexis of the Pütürge metamorphic massive in consequence of crustal thickening. The second stage (Middle Miocene) volcanism was related to continental uplift and lithospheric stretching and triggered the partial melting of the mantle beneath the Anatolian crust. Hence, mantle-derived basaltic melts intruded in Anatolian lower crustal levels, and led to the generation of felsic magmas as the second stage of volcanism, according to Yılmaz et al. (2007). Early to Middle Miocene volcanic activity in this region (called Eastern Anatolian Accretionary Complex, EAAC) was observed in the Elazığ-Tunceli region (Pertek and Mazgirt area; Di Giuseppe et al., 2017; Karaoğlu et al., 2017, 2020) and the Sivas-Malatya region (Yamadağ and Kepez Dağ, Kürüm et al., 2008; Ekici et al., 2009; Ekici, 2016). They are ranging in composition from basalt to dacite-rhyolite, with a calc-alkaline affinity (e.g., Agostini et al., 2019). Ekici (2016) concluded that the Middle to Upper Miocene andesitic-dacitic rocks from Kepez district of Malatya (Eastern Anatolia) are products of heterogeneous mixing between basic end-member magmas and dacitic magmas which are the products of partial melting of lower crustal compositions. The author also suggested that the Kepez volcanic rocks were produced by the collision between Arabian and Anatolian Plates and slab break-off-related uplift of the Eastern Anatolia region. Di Giuseppe et al. (2017) concluded that the volcanic sequence in the Elazığ-Tunceli Region was formed through three different phases. In the first phase Early-Middle Miocene (16.3–15.5 Ma) calc-alkaline basaltic trachyandesitic to dacitic rocks, in the second phase the Late Miocene (11.4–11.0 Ma) transitional basalts, and the latest phase Plio-Pleistocene (4.1 Ma in Karakoçan area and 1.7 Ma in Elazığ area) Na-alkaline basalts erupted. They suggested that the early phase of the volcanism with arc-signature is related to active subduction, and the following phase is associated with the middle Miocene to Recent strike-slip dynamics induced the formation of tears in the subducting slab, local subslab mantle upwelling, and the formation of pull-apart basins. For the Neogene Yamadağ volcanic rocks located between Sivas and Malatya in Eastern Anatolia (Yalçın et al., 1998; Kürüm et al., 2008), Kürüm et al. (2008) stated that Middle Miocene volcanic rocks are characterized by some

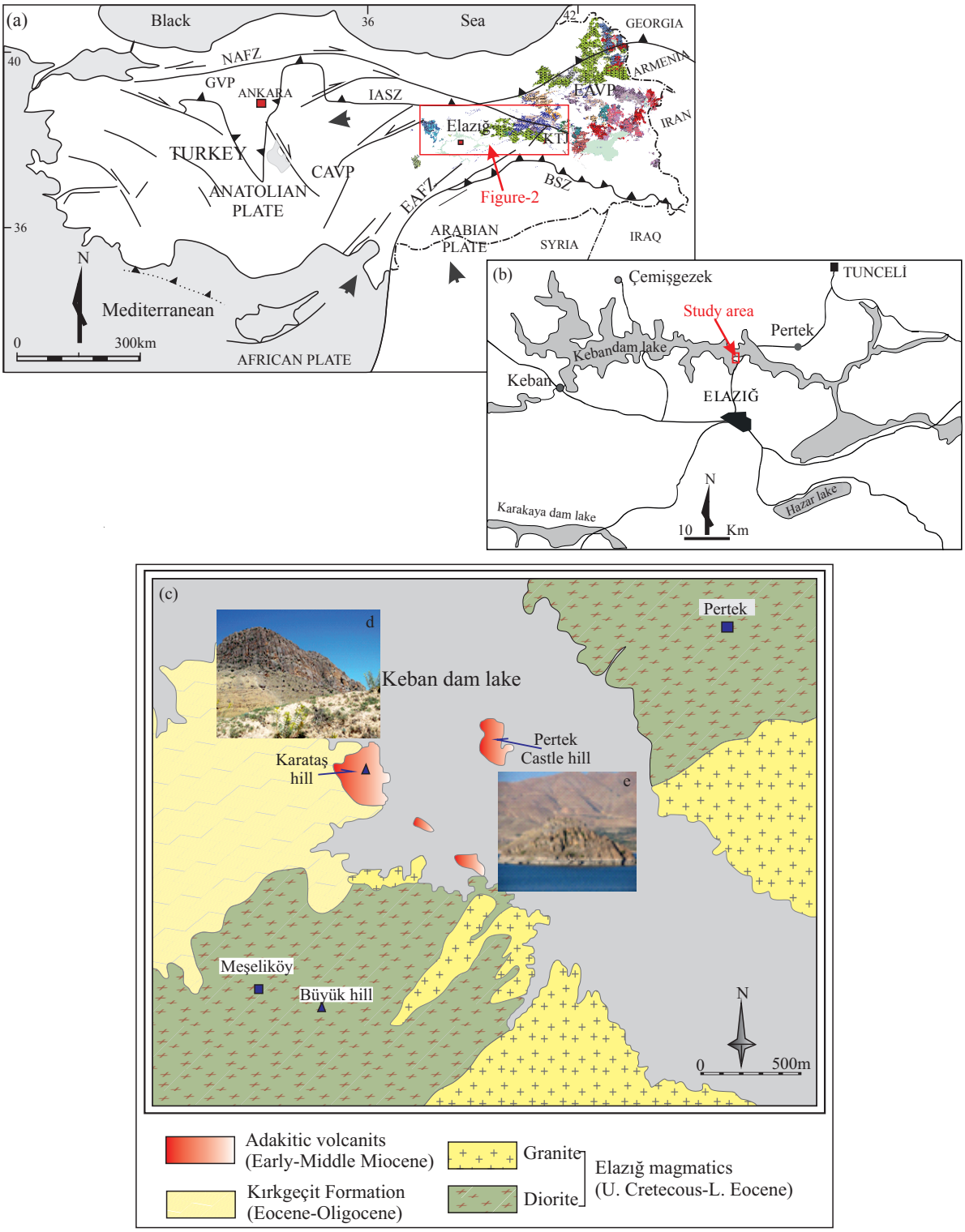

Figure 1. (a) General tectonic map of Turkey, with main blocks (modified from Göncüoğlu, 2010) and Miocene to Quaternary volcanic rocks in the East Anatolian Volcanic Province (EAVP) (modified from MTA, 2002). (b) Location map of the study area. (c) Geological map of the study area and field observations. (d) Adakitic volcanits in Pertek Castle on the island and (e) field observations adakitic volcanits and Kırkgeçit Formation on the Karataş hill. NAFZ-EAFZ; North and East Anatolian Transform Fault; BSZ; Bitlis Suture Zone, KTJ; Karlıova Triple Junction, GVP; Galatya Volcanic Province, IASZ; İzmir-Ankara Suture Zone. Arrows indicate direction of plate movements.

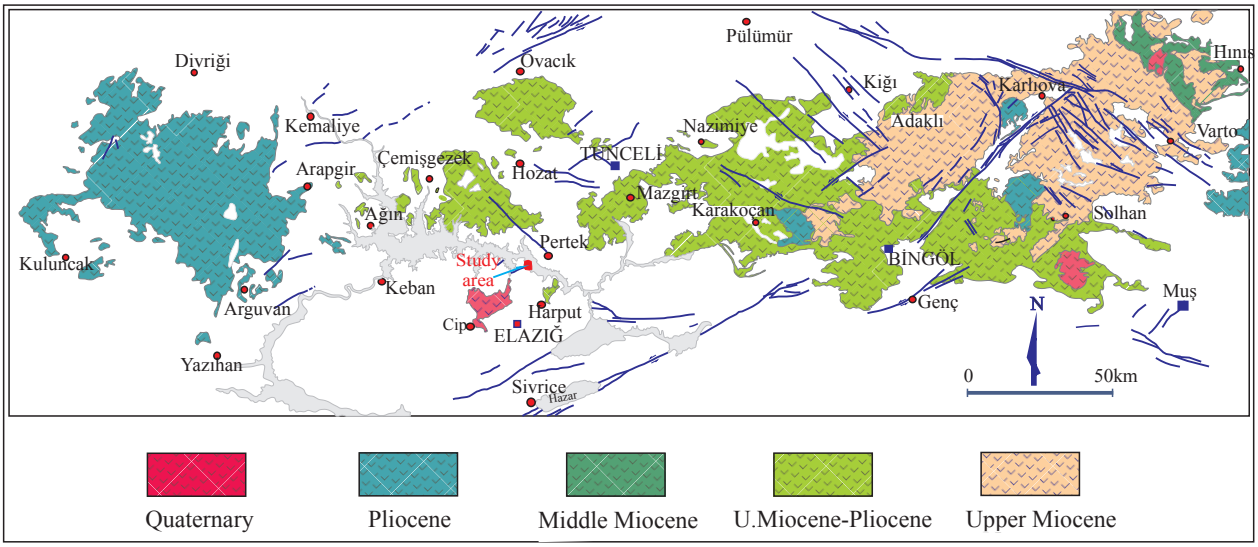

Figure 2. Neogene aged volcanic rocks araound the study area (Kuluncak-Malatya to Hınıs-Erzurum) (modified from MTA, 2002).

small outcrops of basaltic-andesitic-dacitic rocks, overlain upward by basaltic and dacitic rocks, and finally by basaltic lava flows in the Arapkir area, northern Malatya Province. They suggested that these coeval magmas were generated in a postcollisional extensional geodynamic setting in the region. Accordingly, for Miocene to Quaternary volcanic rocks, ranging from alkali basalt to rhyolite, in the Karlıova-Varto region in the East Anatolia, Karaoğlu et al. (2017, 2020) concluded that they are triggered by active lithosphere passive asthenospheric mantle, and associated with lithospheric thinning and uplift-related inversion tectonics (reactivation of preexisting faults), and mainly dominated by subduction-related signatures, with most of the primary magma characteristics having been masked by fractionation and crustal assimilation processes.

3. Brief geology and volcanic setting in Pertek (Tunceli) area

The study area is located in a collisional zone that occurred between Arabian and Anatolian plates in Eastern Anatolia (Figures 1a and 1b). The basement association in the area is made up of the Late Cretaceous, subalkaline magmatic rocks known as Elazığ magmatics/Yüksekova Complex (Sağıroğlu and Şaşmaz, 2004; Rızaoğlu et al., 2009; Kürüm et al., 2011; Parlak et al., 2012; Ural et al., 2015). They are characterized mostly by granite and diorite plutons and microdiorites, basaltic lavas, and pyroclastic rocks. Felsic and mafic dykes are observed as intrusions in the plutonic rocks (Herece and Acar, 2016). Middle Eocene volcanism in the surrounding region was recorded in Maden Complex situated from Bitlis-Zagros Suture Zone (Ertürk et al., 2017). In the NW of Pertek area, the Paleogene units start with the Middle Eocene and Late Oligocene Kırkgecit Formation (conglomerate and marine sediments), overlain by the Oligocene-Early Miocene Alibonca Formation (conglomerates, shallow marine carbonates, and sandstones) (Aksoy et al., 2005). Continental sediments (conglomerates and sandstones) are followed by lacustrine deposits of the Karabakır Formation. Obtained Ar-Ar geochronological determinations (16.25 Ma for andesite, 15.75 Ma for dacite and 15.52 Ma for basaltic andesite, Di Giuseppe et al., 2017) from the porphyries cropping out into the NW of Pertek area give Early to Middle Miocene age for Pertek volcanic rocks. In the study area (SW of Pertek), the Middle Eocene-Late Oligocene Kırkgeçit Formation, overlying the basement magmatic association, reaches up to 250 m-thickness and forms the lower part of Middle Miocene adakitic porphyries. The unit is dominated by conglomerates, sandstones, siltstones, and limestones and shows typical characteristics of flysch facies deposits (Özkul, 1988). The Kırkgeçit Formation is characterized by gently dipped, laterally discontinuous coarse sandstone beds (Figures 1c and 1e) and forms a peneplain topography. The Pertek SW porphyries studied appear in the Keban dam lake and along the shore and, show columnar jointing (Figures 1c and 1e).

4. Analytical methods

For petrographical, mineral chemical, and bulk chemical analysis, representative fresh samples were collected from the studied volcanic rocks. Whole-rock analyses have been performed at the ACME-Analytic Laboratories (Canada) by ICP-AES (major and some trace elements) and ICP-MS (some trace elements and REEs). To determine the whole-rock chemical (major, trace, and rare earth element) analyses compositions, 0.2 g samples of rock powder

were fused with 1.5 g $Li_2B_4O_7$ and then dissolved in 100 mL 5% HNO_3. Loss on ignition (LOI) was determined by weight difference after ignition at 1000 °C. Detection limits range from 0.002 to 0.04 wt.% for major oxides, 0.1 to 8 ppm for trace elements, and 0.01 to 0.1 ppm for the rare earth elements (REE). Six samples were chosen for microchemical analysis, and were performed, along the long axis of the crystals, at the Electron Microscope and Microanalyses Laboratory of the Geological Engineering Department of Hacettepe University (Ankara, Turkey), using a Bruker-Axs Quantax XFlash 3001 EDS integrated with a Zeiss Evo-50 EP microscope. Accelerating voltage and beam current was 15 kV and 15 nA, with 45 sn and 10 mm counting times respectively.

5. Results and discussion

5.1. Petrography and spot-analyses of phenocryst phases

Pertek volcanic rocks with 25% to 60% phenocrysts show porphyritic texture. Phenocrystal associations are dominated by plagioclase accompanied by sanidine, biotite, quartz, and amphibole in lesser amounts. Fe-Ti oxide, sphene, and zircon are present as accessory minerals. In the microcrystalline matrix, sericitization, carbonation, and silicification are the common alteration types. Plagioclase phenocrysts are from euhedral to subhedral in shape and vary in length. They are strongly altered and show chemical zoning and twinning (Figure 3a). Rare sanidine phenocrysts are strongly altered and contain plagioclase inclusions, and similar to plagioclase crystals, show dissolution texture in places (Figure 3b). Quartz crystals are in varying sizes, rounded and embayed along their crystal surfaces (Figure 3c). Generally, euhedral and prismatic biotite crystals form almost 10% of the phenocryst association. Biotite microcrystals, on the other hand, are found as thin prismatic laths or bladed in shape. Phenocrysts biotites exhibit strong chloritization while microlites are fresh. Amphibole phenocrysts are generally euhedral (Figure 3d) or found as pseudomorphs.

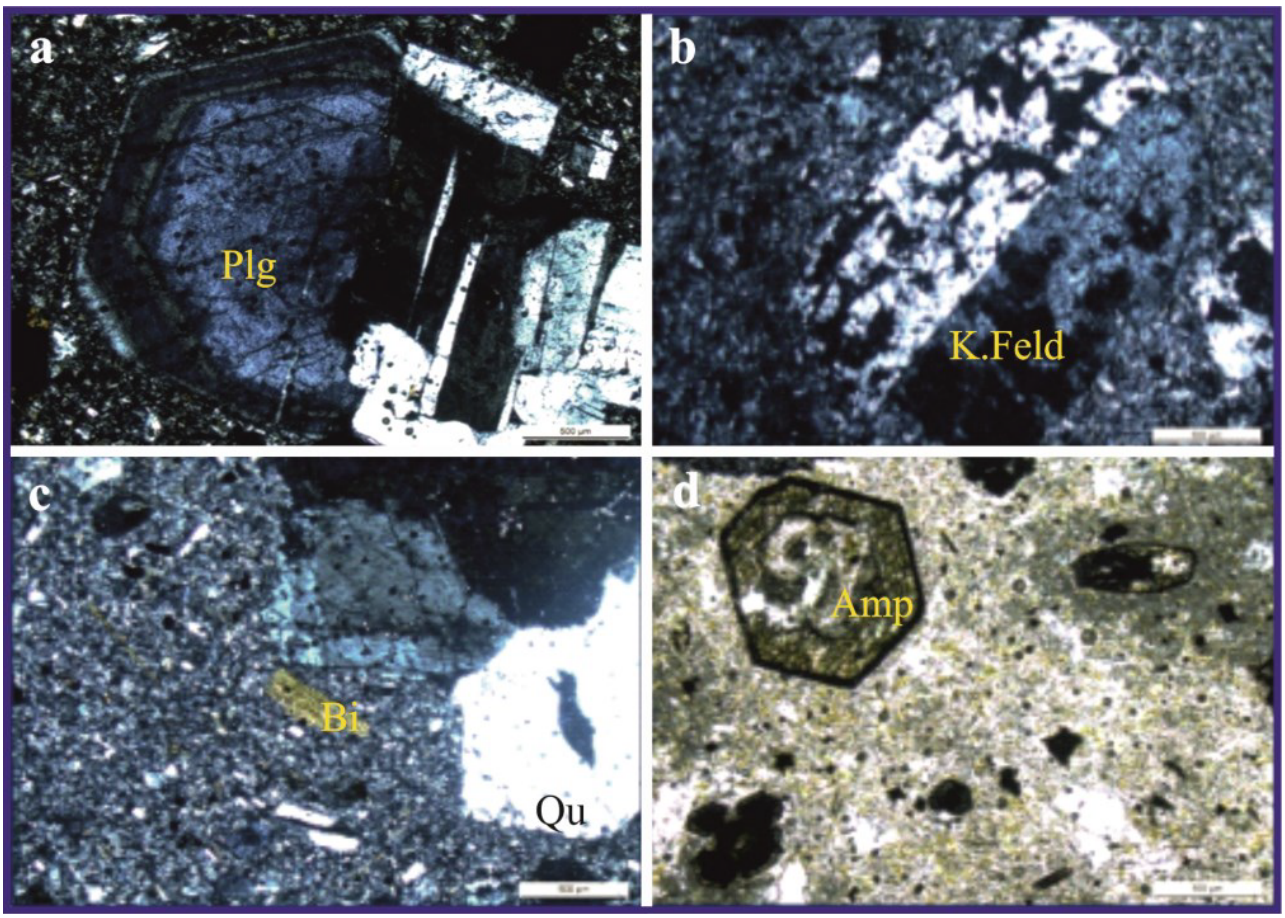

Figure 3. Microphotographs showing textural features of the adakites. (a) Plagioclase with zoning in microlitic porphyritic dacite, (b) Embayed K-feldspar phenocrystal, (c) Quartz, plagioclase and biotite phenocrysts in fine-grained with felsic mineral matrix, (d) Hornblendes in porphyritic texture (parallel light). Plg; Plagioclase, K.Feld; K-Feldispar, Bi; Biotite, Qu; Quartz, Amp; Amphibole. The scale bars on the photomicrographs are 500 micrometer.

Plagioclase phenocrysts from five samples (P2, P6, P9, P11, P19) in the Pertek volcanic rocks were chemically investigated, and 19–25 spots in each plagioclase crystal were analysed (Appendix Table 1). Plagioclases are geochemically oligoclase to labradorite in composition (Figure 4a). In andesites, plagioclase phenocrysts are $An_{24-57}Ab_{28-74}Or_{1-5}$ in composition while in dacite samples, Na-rich plagioclase crystals of oligoclase and andesine with the composition of $An_{21-35}Ab_{58-77}Or_{2-5}$ are common (Figure 4a; Appendix Table 1). Chemical compositions of biotite crystals from four different samples (P9, P11, P19, P20) have distinct Fe^{2+}/ (Fe^{2+} + Mg) and total Al and Mg contents (Figure 4b). In samples, total Al ranges from 0.94 to 1.63 apfu (atoms per formula unit), Fe^{2+}/ (Fe^{2+}+ Mg) from 0.41 to 0.78 and total Mg from 0.54 to 1.58 apfu (Appendix Table 2). However, a weak negative correlation between Fe and Al is observed (Figure 4b). Total Al-Fe^{2+}+/(Fe^{2+}+Mg) content of biotites, plotted in the annite–phlogopite–siderophyllite–eastonite quadruple diagram, show that they are lepidomelane and meroxene in composition (Guidotti, 1984; Figure 4b). Amphiboles from two samples (P9, P11) were chemically examined (Appendix Table 3). They generally have high Ca (0.95–3.52 and 0.76–2.02 apfu), Mg (0.63–3.42 and 1.00–2.42 apfu), and Al (1.53–6.18 and 1.22–2.69 apfu) contents indicating that they are calcic amphiboles (hornblende) in composition (Hawthorne, 1983). Silica contents of the amphibole crystals from Pertek volcanic rocks are lower than 7.50 apfu, indicating that they are magmatic amphiboles (Leake, 1971) and dominantly pargasite, ferropargasite in compositions (Figure 4c).

5.2. Geochemistry

Major and trace element composition of analysed thirteen samples from Pertek volcanic rocks are given in Table 1. Since their proximity and similar geochemical affinity, studied rocks are evaluated together with coeval generated andesite-dacite porphyries from N of the Pertek area (Di Giuseppe et al., 2017). In the analysed samples, SiO_2 content varies from 61.79 up to 66.40 wt.%, Al_2O_3 from 16.19 to 17.94 wt.%, and MgO from 0.93 up to 1.56 wt.%. All samples from the intermediate to acidic volcanic rocks in Pertek area show subalkaline chemical affinity in total alkalies (TAS) versus silica diagram and are high-K calc-alkaline andesite and dacite in compositions (Figures 5a and 5b). Relatively high LOI (1.3–3.3%), Na_2O (4.05–4.63 %) and Na_2O/K_2O (1.37–1.68 %) values indicate that these rocks originated from compositionally differentiated magmas or they differentiated through post eruptional processes. Contrary to the Pertek northern porphyries with high Mg# (ranging between 59 and 65), Cr (30–270 ppm) and Ni (30–110 ppm) contents (Di Guiseppe et al., 2017), southern porphyries studied have low Mg# (Mg/ $Mg+Fe_{TOT,}$ ranges from 30 to 40), Ni (1.8–4.3 ppm) and Cr (up to 20 ppm) contents. Relatively high K_2O (2.57–3.05 wt.%), Th (11.7–12.8 ppm), Rb (90.1–110.9 ppm), Hf (3.9–4.8 ppm), Ba (520–596 ppm), Sr (412–637 ppm), and Zr (149–180 ppm) contents are also their characteristic feature. Respectively, Sr, Y and Yb contents of Pertek rocks (Sr, 412–637 ppm; Y, 7.3–10.5 ppm and Yb, 0.40–0.73 ppm) coincide with typical adakites having high Sr (>400 ppm) and low Y (<20 ppm) and Yb (<2.0 ppm) values. The adakitic nature of southern and northern porphyries of Pertek volcanic rocks is also clear in Sr/Y versus Y (Defant and Drummond, 1990; Castillo, 2012) and La/Yb versus Yb (Castillo, 2012) diagrams (Figures 6a and 6b). In the primitive mantle-normalized multielement diagram, they are characterized by negative Nb-Ta and Ti anomalies (Figure 7a), and in the chondrite normalized spider diagram, they show enrichment in the LILE and LREE over HREE and show slightly negative Eu anomaly (Figure 7b), which are similar to those of metasomatized mantle-derived Iranian Azerbaijan Middle Miocene-Quaternary adakite-like andesites and dacites (Lechmann et al., 2018). In these multielement diagrams, it is seen that Malatya (Yılmaz et al., 2007) and Pertek samples (Di Giuseppe et al., 2017) are also similar to one another.

5.3. Significance of mineral phases

Plagioclase and mafic phenocrysts phases (amphibole, biotite) in porphyritic Pertek andesites-dacites are identical to adakitic magmas. Amphiboles are the first mineral phase to crystallize in most adakitic magmas (Prouteau and Scaillet, 2003; Tang et al., 2017). Amphiboles, examined in this study are Al-rich (Al_2O_3 up to 15.94 wt.%), which is pressure sensitive component of amphiboles. As shown in Figure 8a, plots of the Al content against Mg#, overlap close to the high-pressure amphibole compositions obtained by Alonso-Perez et al. (2009), in the range 800–1200 MPa and high water content (4–8 wt%). Thus the most likely interpretation is that these minerals appear as one of the first phases, having crystallized at high pressures. This is consistent with the mafic lower crustal melting model, rather than a high-pressure basaltic melt fractionation, for adakite petrogenesis (c.f., Tang et al., 2017). Tang et al. (2017) concluded that melting of thickened lower crust can produce pristine adakitic magma, regardless of whether or not the adakitic magmas were produced via crystallization. Lower crust-derived adakitic rocks have the potential for tracing the time at which thick continental crust is developed in settings such as the Tibetan plateau (Chung et al., 2003; Wang et al., 2005) or the Andes in South America (Goss and Kay, 2009). In other words, biotite crystals in Pertek rocks are more ferroan than magnesian and peraluminous in composition. They display consistency with the micas from crustal xenoliths with the higher Al_2O_3 contents. However, the FeO_T / (FeO_T + MgO) vs. MgO diagram (Zhou, 1986) suggests that

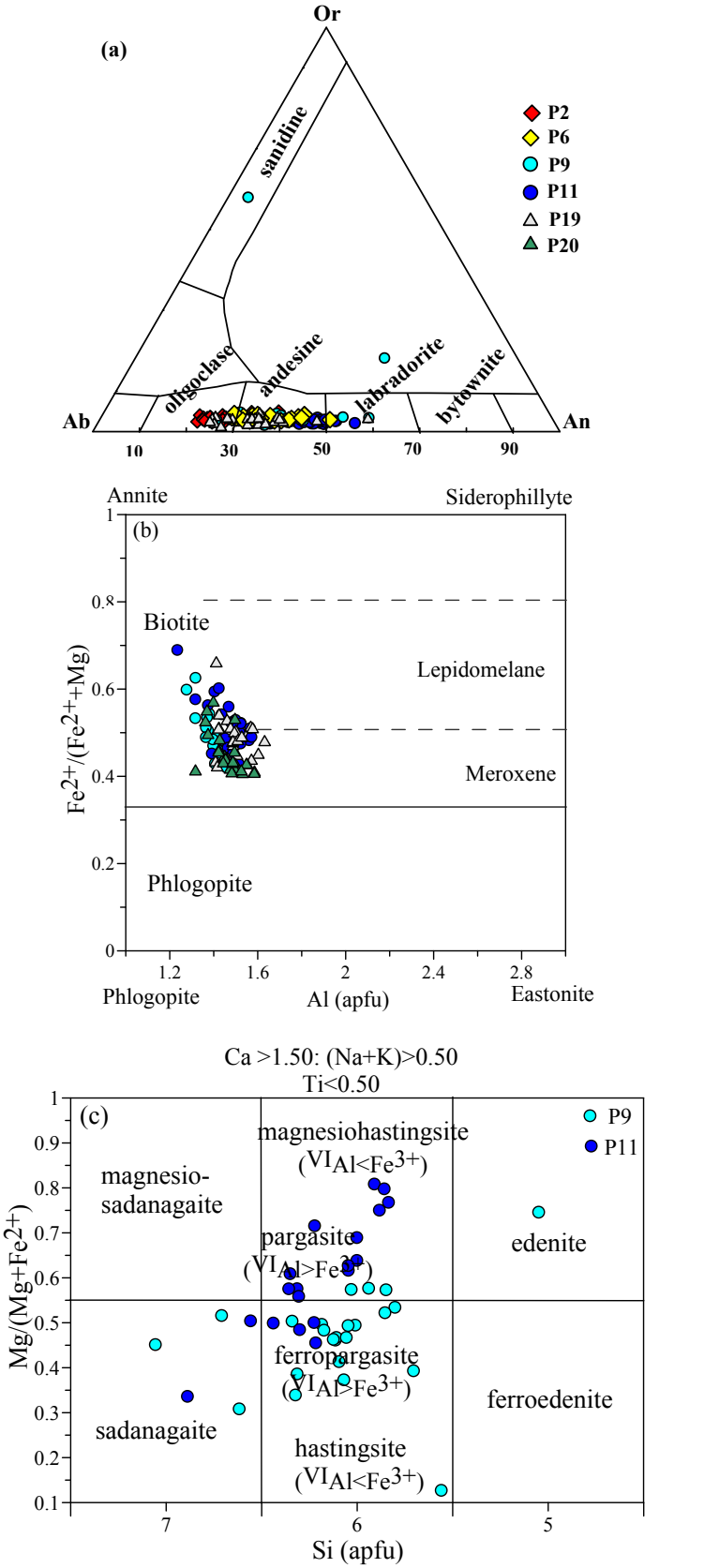

Figure 4. Mineral phase composition of (a) feldspars, (b) biotite and (c) amphiboles of samples analysed by EMPA.

Table. Whole rock major and trace element analyses of the Pertek adakitic rocks.

Sample	P-2	P-6	P-9	P-11	P-13	P-14	P-16	P-18	P-19	P-20	P-21	P-22	P-23
SiO2	63.57	61.79	63.69	63.33	64.11	66.40	63.45	64.00	64.99	65.05	63.58	63.63	64.41
TiO2	0.60	0.61	0.58	0.55	0.47	0.51	0.57	0.53	0.56	0.56	0.56	0.58	0.58
Al2O3	16.93	17.94	17.65	17.31	16.19	16.47	16.83	16.84	17.19	17.32	16.84	17.89	17.01
Fe2O3	3.79	3.75	3.51	3.39	2.79	2.98	3.49	3.55	3.20	3.21	3.45	3.49	3.47
MnO	0.05	0.04	0.04	0.03	0.03	0.03	0.04	0.04	0.03	0.03	0.04	0.02	0.03
MgO	1.56	1.41	1.32	1.29	1.08	1.12	1.38	1.20	1.04	1.07	1.30	0.93	1.19
CaO	3.84	3.57	3.90	4.69	4.98	3.35	3.89	4.20	3.65	3.76	4.17	3.85	3.63
Na2O	4.33	4.35	4.54	4.61	4.05	4.17	4.41	4.34	4.36	4.46	4.35	4.63	4.45
K2O	2.57	2.83	2.92	2.84	2.70	3.05	2.66	2.82	2.93	2.82	2.66	2.80	2.79
P2O5	0.21	0.19	0.20	0.19	013	0.14	0.19	0.18	0.22	0.18	0.20	0.19	0.18
LOI	2.3	3.3	1.4	1.6	33	1.6	2.9	2.1	1.6	1.3	2.6	1.8	2.1
Total	99.79	99.79	99.77	99.79	9980	99.79	99.79	99.79	99.80	99.78	99.80	99.79	99.80
Sc (ppm)	5.00	4.00	4.00	4.00	3.00	3.00	4.00	4.00	4.00	4.00	4.00	4.00	4.00
Ba	527	530	571	542	544	596	536	543	510	553	521	556	520
Be	3.00	3.00	2.00	2.00	2.00	<1	3.00	3.00	3.00	2.00	<1	4.00	1.00
Co	7.50	6.80	6.10	5.90	4.40	5.40	6.30	6.00	5.40	5.90	6.50	6.90	6.40
Cs	8.50	3.60	3.70	2.60	3.20	4.00	3.80	3.50	3.70	3.20	3.60	3.60	3.30
Ga	19.80	20.70	21.20	19.90	19.00	20.10	19.90	19.80	20.50	20.40	20.50	22.50	19.20
Hf	4.50	4.70	4.80	4.00	4.30	4.30	4.30	4.10	4.40	4.40	4.40	4.50	3.90
Nb	9.80	9.70	9.30	8.90	7.90	8.60	9.40	8.40	8.70	8.80	9.10	9.50	8.90
Rb	90.10	98.50	101.00	97.30	98.00	110.90	92.80	92.40	99.10	92.30	93.10	98.30	93.50
Sn	1.00	2.00	2.00	2.00	2.00	2.00	2.00	2.00	2.00	2.00	2.00	1.00	1.00
Sr	437	448	637	466	413	412	450	440	433	548	441	474	425
Ta	0.70	0.70	0.70	0.70	0.60	0.70	0.60	0.70	0.60	0.60	0.70	0.70	0.70
Th	12.10	12.60	12.70	1210	12.00	11.80	12.40	12.10	12.00	11.70	11.70	12.70	12.80
U	3.70	3.90	3.80	3.50	3.80	3.60	3.30	3.40	3.50	3.60	3.40	3.80	3.30
V	56.00	49.00	50.00	51.00	52.00	52.00	48.00	48.00	48.00	46.00	46.00	51.00	49.00
W	0.50	0.50	0.50	<0.5	1.00	0.60	0.70	<0.5	0.60	0.70	0.70	1.10	1.70
Zr	176	180	177	168	149	168	168	165	165	156	162	170	165
Mo	0.50	0.20	0.20	0.20	0.10	<0.1	0.50	0.30	0.20	0.20	0.40	0.20	0.40
Cu	9.80	8.70	8.40	8.00	4.90	4.90	780	7.30	7.30	6.30	7.20	6.50	7.20
Pb	1.10	1.90	120	0.90	1.60	1.20	1.30	1.10	1.10	1.20	1.00	0.80	0.90
Zn	47.00	51.00	34.00	29.00	35.00	38.00	45.00	29.00	23.00	25.00	33.00	29.00	27.00
Cr	20.53	6.84	20.53	13.68	6.84	6.84	6.84	6.84	13.68	20.53	20.53	6.84	6.84
Ni	4.30	3.70	3.10	2.60	1.80	1.90	3.70	3.10	3.80	3.30	3.50	3.50	2.90
Y	10.10	10.50	9.10	8.40	7.30	7.30	9.70	9.10	8.80	8.90	8.60	9.00	8.30
La	29.20	29.70	29.30	27.70	24.50	25.20	28.60	28.20	26.50	27.20	27.70	30.90	28.10
Ce	54.40	54.20	55.70	51.50	46.90	46.70	51.70	53.50	50.80	50.10	53.20	57.50	51.40
Pr	6.00	6.05	5.90	5.68	5.15	5.22	5.94	5.64	5.61	5.61	5.67	6.32	5.84
Nd	21.50	21.50	21.90	20.30	19.30	18.40	23.00	20.00	20.50	20.40	21.20	21.30	20.50
Sm	3.71	3.90	3.99	3.57	3.48	3.64	3.92	3.59	3.62	3.68	3.69	3.88	3.48
Eu	1..04	1.05	0.98	0.95	0.89	0.91	1.00	0.91	0.95	0.98	0.94	1.05	0.95

Table. (Continued).

Gd	3.30	3.34	2.99	3.00	2.79	2.87	3.21	2.96	3.08	3.04	3.25	3.48	3.24
Tb	0.40	0.41	0.36	0..36	0.33	0.33	037	0.37	0.36	0.35	0.38	0.40	0.36
Dy	2.21	2.42	2.00	1.85	1.75	1.90	1.89	2.03	1.85	1.89	1.91	2.16	1.88
Ho	0.35	0.35	028	0.32	0.21	0.24	0.30	0.28	0.29	0.27	0.30	0.30	0.30
Er	0.85	080	0.66	0.67	0.50	0.53	0.74	068	0.75	0.70	0.75	0.76	0.72
Tm	0.12	0.12	0.10	0.09	0.07	0.07	0.11	0.10	0.09	0.09	0.09	0.10	0.10
Yb	0.73	0.69	0.64	0.52	0.40	0.42	0.62	0.64	0.55	0.56	0.60	0.64	0.53
Lu	0.11	0.11	0.09	0.08	0.06	0.06	0.11	0.09	0.08	0.08	0.09	0.09	0.08
Eu/Eu*	0.89	0.87	0.83	0.86	0.84	0.83	0.84	0.83	0.85	0.87	0.81	0.86	0.85
Mg#	39.48	37.34	37.34	37.62	38.02	37.33	38.52	34.88	33.99	34.56	37.39	29.69	35.21

"STD SO-18, STD OREAS45EA" the standards were used in the production of the analysis whole rock major and trace elements.

some of the Pertek micas were derived from a crust-mantle mixed source while some are originated from a mantle source region (Figure 8b).

5.4. Geochemical remarks of hybrid source for Pertek adakitic rocks

One of the suggested models for acidic magma formation is the melting of the crust, via a thermal source supplied by mantle-derived basaltic magma (Bullen and Clynne, 1990). Thus, acidic magma could be derived from partially melted mafic-intermediate metamagmatic rocks (Rapp and Watson, 1995) or metasedimentary rocks (Patiño Douce and Beard, 1996). This model resembles that of crust-derived (continental) adakites (e.g., Wang et al., 2005; Liu et al., 2008; Deng et al., 2018; Karslı et al., 2019, 2020). However, it was also suggested for these types of adakites that, they originated from high-pressure fractional crystallization of hydrous basaltic melt (Macpherson et al., 2006) or crustal assimilation of magma and low-pressure fractionation (Castillo et al., 1999). The high-pressure fractional crystallization of hydrous basaltic melts with garnet shows a regular geochemical pattern such as decreasing Al_2O_3 and La contents with decreasing SiO_2, and the increasing Sr/Y ratios with increasing SiO_2 (Prouteau et al., 2001; Macpherson et al., 2006), which is observed in Pertek adakitic porphyries (Figures 9a–9f). High-pressure (garnet and amphibole) fractional crystallization of hydrous basaltic melts is suggested for the generation of the adakitic lavas in the studied area. A garnet-bearing amphibolitic source domain during partial melting requires at least greater than 40 km depth (>1.2 GPa) (Rapp and Watson, 1995; Petford and Atherton, 1996; Azizi et al., 2019). Hence, the crustal thickness of Eastern Anatolia High Plateau (EAHP), geologically located on the East Anatolian Accretionary Complex (Şaroğlu and Yılmaz, 1987) was likely greater than 40 km (approx. 45 km, Şengör et al., 2003) when the Pertek adakitic magmas were formed in Early to Middle Miocene. During partial melting of hydrous basalt under amphibolite or eclogite facies conditions, garnets are in the relict phase and stable while plagioclases are not (Rapp et al., 1991; Şen and Dunn, 1994; Rapp and Watson, 1995). Adakitic magma could be produced from the lower part of the thickened crust, or basaltic parts of the subducted oceanic crust. These kinds of magmas have high Sr, low Yb, MgO, Cr, Ni contents, and low Mg number (<40–45) (Defant and Drummond, 1990; Şen and Dunn, 1994; Rapp and Watson, 1995; Petford and Atherton, 1996). Experimental studies show that melting of the mafic crustal rocks, in proper depths (>40 km, approximately 1.2 GPa), may produce adakitic liquids (e.g., Rapp et al., 2003 and references therein). Since their low MgO (up to 1.50 wt.%), Cr (up to 21 ppm), and Ni (<4.30 ppm) contents, Pertek adakitic rocks cannot be sourced solely from partial melting of lithospheric mantle in garnet stability conditions. Supporting this model, the 10–15% garnet-amphibole-bearing partial melting curve of these adakites shows a close correlation with the eclogite curve (Figure 7b) and is similar to classic adakites. Thus, the chemical characteristics of the Pertek adakites suggest a garnet and amphibole-bearing lower crustal source. A similar situation is observed in NW Iran adakitic granitoids produced by amphibole-dominated fractionation of hydrous melts of subcontinental lithospheric mantle accompanied by minor assimilation of lower continental crust (Azizi et al., 2019). These results may also indicate mixing of melts derived from the mafic continental crust and subducting slab (Kamvong et al., 2014), or mixing of melts derived from the mafic lower crust and metasomatized mantle (Guo et al., 2007).

The geochemical characteristics of Pertek adakitic porphyries resemble those of high silica adakites (HSA) (Martin et al., 2005) (Figure 10a). These porphyries with low Mg# (30–40) have contents of high K_2O (2.57–3.05

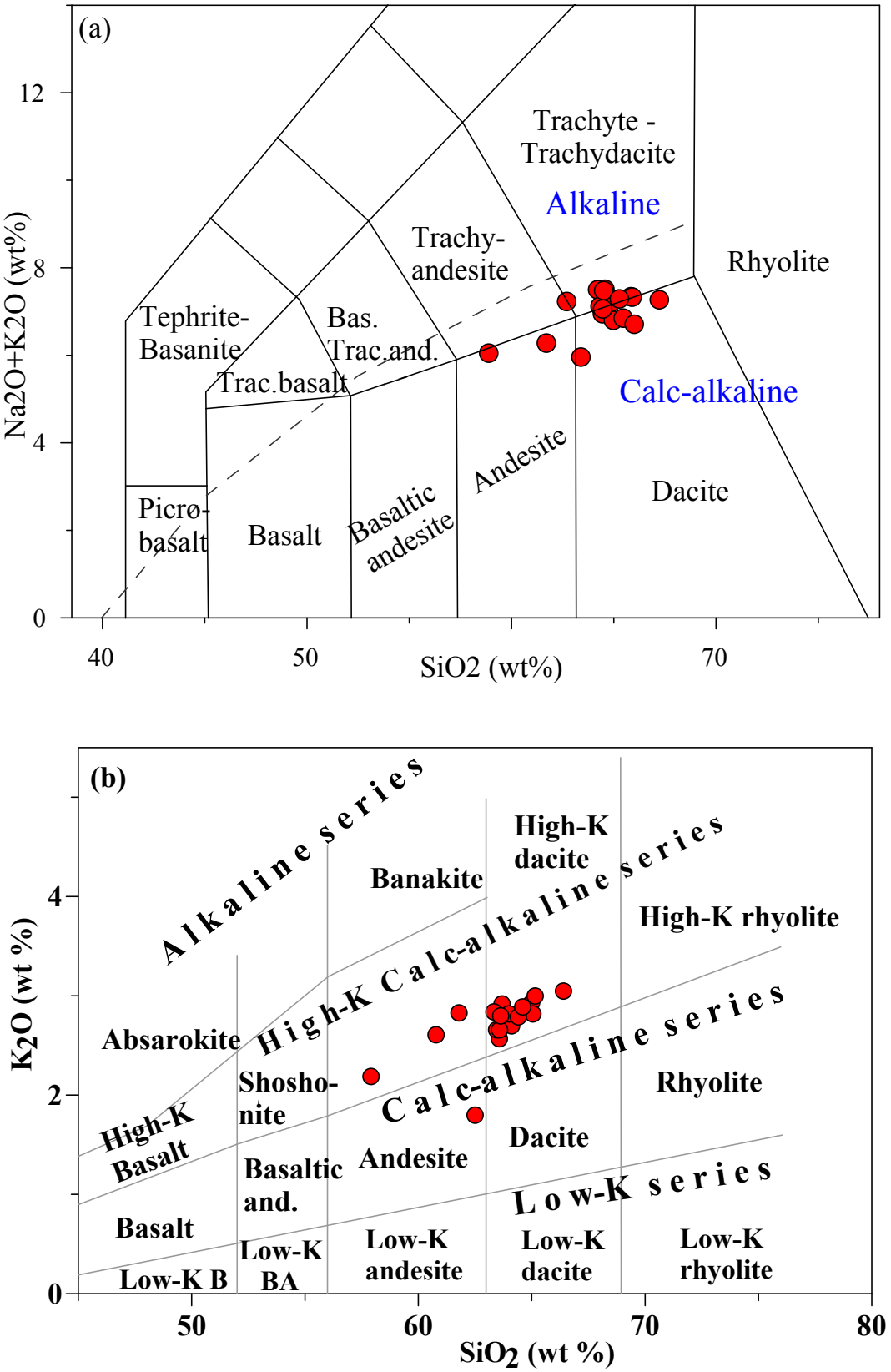

Figure 5. (a) Classifications of the Pertek volcanics on the TAS diagram (Le Maitre et al., 2002), and (b) K_2O-SiO_2 diagram (Peccerillo and Taylor, 1976).

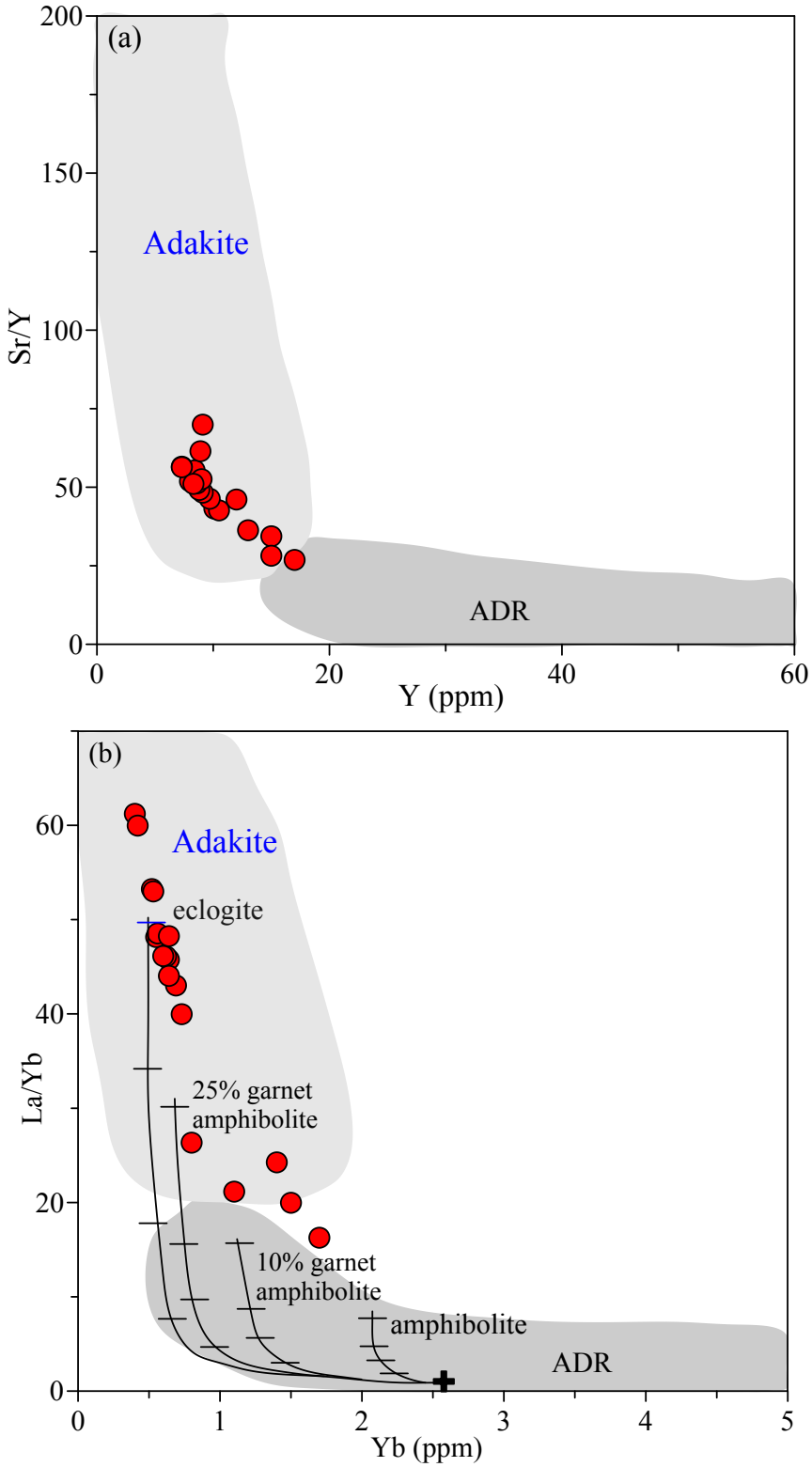

Figure 6. (a) Sr/Y vs. Y variations for Pertek andesite-dacite porphyries to distinguish adakite from normal arc ADR (Andesite-Dacite-Rhyolite) volcanic rocks (Defant and Drummond, 1990 and Castillo, 2012), (b) La/Yb ratios vs. Yb variations for Pertek porphyries (Castillo, 2012, references therein). Northern Pertek dacitic rocks (Di Giuseppe et al. 2017) are included in Pertek data. The curves generally show that high Sr/Y and La/Yb magmas can be produced through partial melting of eclogite and garnet-bearing amphibolite sources (Castillo, 2012).

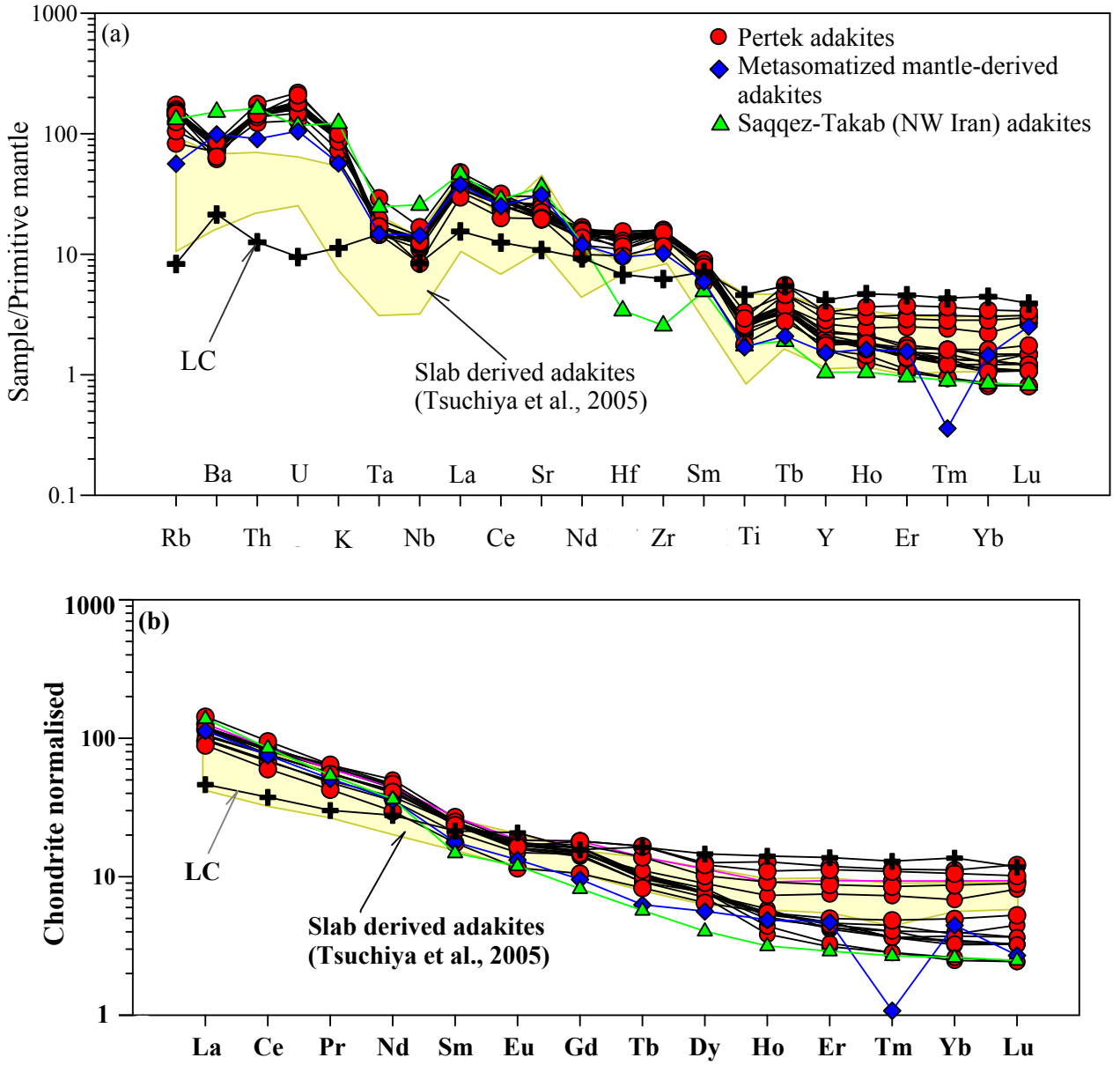

Figure 7. (a) Primitive mantle and (b) Chondrite-normalized multielement diagrams for Pertek andesitic-dacitic porphyries. Northern Pertek andesite-dacite porphyries also included (Di Giuseppe et al., 2017). Normalizing values are from Sun and McDonough (1989). LC (Lower continental crust) values after Rudnick and Gao (2004). Malatya Middle Miocene rhyolites from Yılmaz et al., (2007), metasomatized mantle-derived adakites for the average value of 15 adakite samples after Lechmannn et al. (2018), and Saqqez-Takab (NW Iran) adakitic granitoid for the average value of 12 adakite samples from Azizi et al. (2019).

wt%), and low Cr (<21 ppm), and Ni (<4.30 ppm). In general, their characteristics are comparable with those of the (i) crustal adakites (K-adakites) (Moyen, 2009) or (ii) mafic lower crust-derived adakites (Atherton and Petford, 1993; Wang et al., 2007) (Figure 10b). However, Pertek adakites have high Fe_2O_3 content (2.70–3.79 wt%) (Table). The samples are concentrated in the adakite area derived from the thickened lower crust in the MgO-SiO_2 diagram and are located close to the subduction-related adakitic field (Figure 10b). Similar characteristics are also observed in Iranian-Azerbaijan metasomatized mantle-derived adakitic volcanic rocks (Lechmann et al., 2018) and adakitic Saqqez-Takab pluton (Azizi et al., 2019). The samples plotted in Figures 10b and 10c fall in the overlapping area of different types of adakites and indicate that the formation of the magma that produced the Pertek adakites cannot be explained only by a crustal origin. Hence the origin of the Pertek adakitic rocks could be

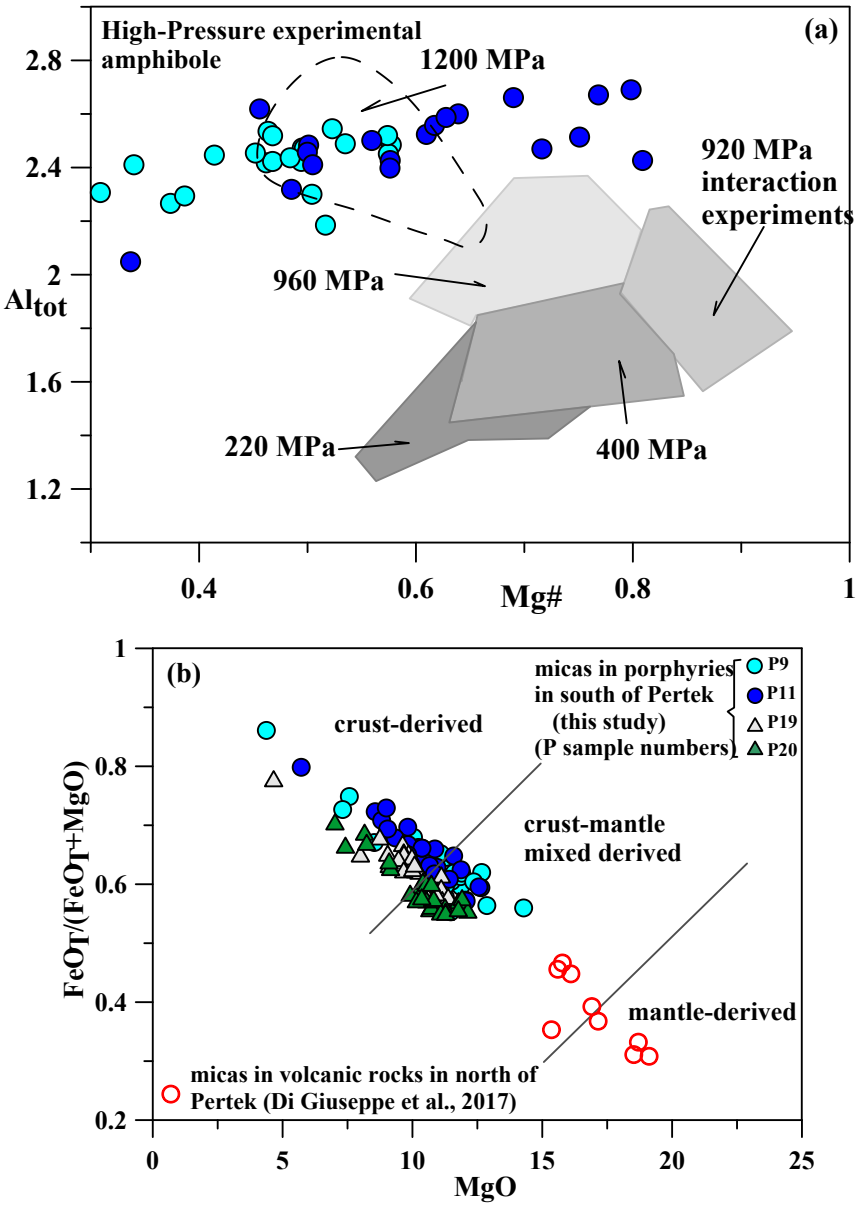

Figure 8. (a) The compositions of amphiboles in the Pertek porphyries are compared with field for natural amphiboles and experimental amphiboles at 220 MPa, 400 MPa and 960 MPa, and andesite at 1200 MPa (after Tang et al., 2017). (b) MgO (wt.%) versus FeO(t)/(FeOt + MgO) diagram (after Zhou, 1986) of micas in Pertek adakitic porphyries.

attributed to both subcontinental lithospheric and lower crustal sources.

Based on the similarities between the geochemical characteristics of adakite magmas and hydrous basaltic magmas obtained from experimental studies, Defant and Drummond (1990) suggested a subducted oceanic crustal origin for classical adakites. However, it was observed in experimental studies that MORB-like melts in, 1–2 GPa and ≤1000 °C conditions, have low K_2O (<1.2 wt %) and K_2O/Na_2O ratios (<0.25) (Rapp et al., 1991; Rapp and Watson, 1995). It is accepted that, relative to those of lower crust-derived adakites, slab-derived adakites are characterized by lower K_2O/Na_2O and higher CaO/Al_2O_3 ratios (e.g., Defant and Drummond, 1990; Li et al., 2016). Hence, the low K_2O/Na_2O (0.59–0.73) and high CaO/Al_2O_3 (0.20–0.27) ratios for the Pertek adakitic andesite-dacites, are located in the overlapping region of the slab-derived origin and lower crust-derived adakitic melts (Figure 11a), whereas nearly coeval Malatya rhyolitic dykes and Giresun adakitic rocks fit in the field of the lower crust-derived adakitic melts. Pertek acidic rocks and central Anatolian adakitic porphyries are also comparable with slab-derived

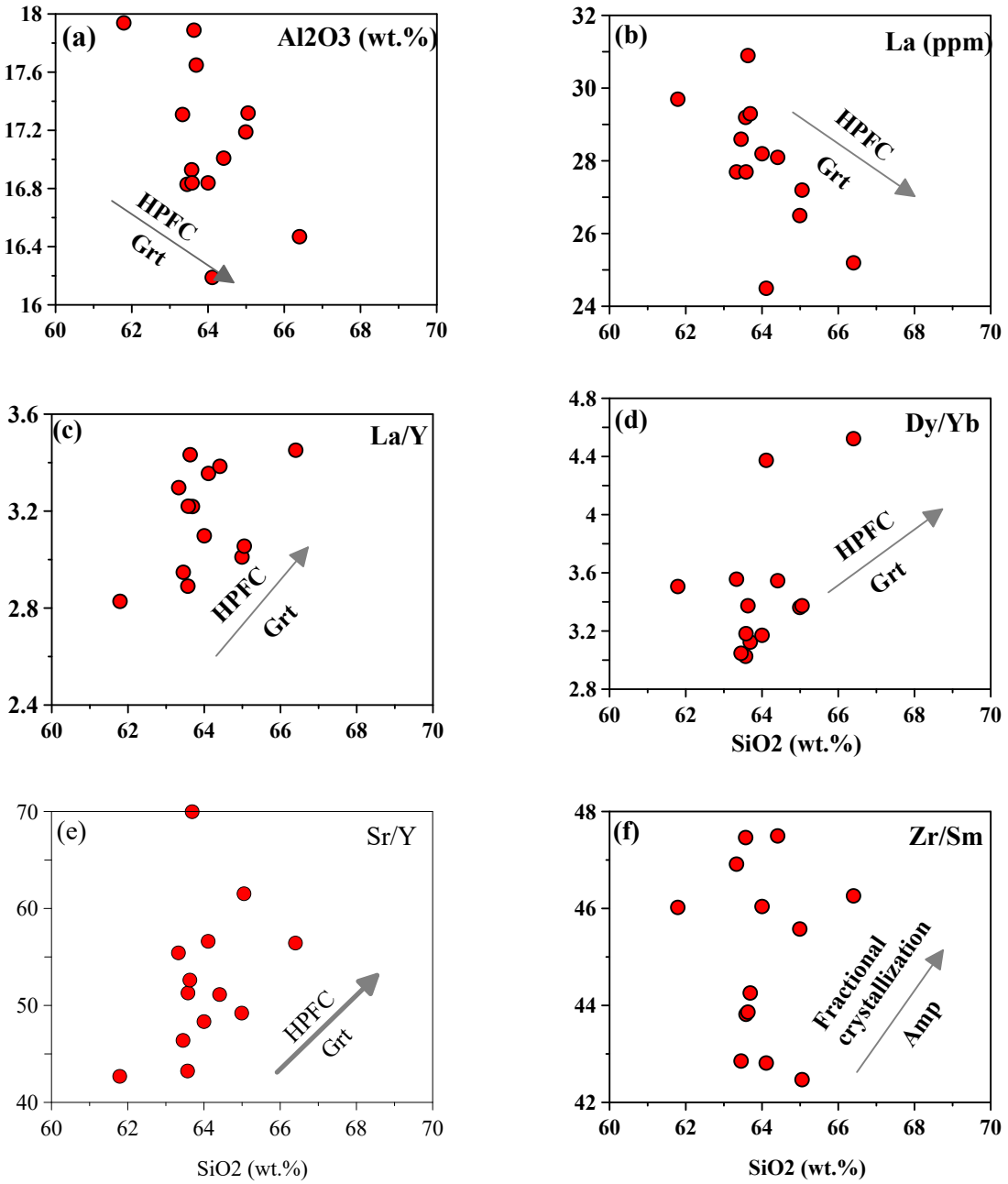

Figure 9. (a) Al_2O_3 vs. SiO_2, (b) La vs. SiO_2, (c) La/Y vs. SiO_2, (d) Dy/Yb vs. SiO_2, (e) Sr/Y vs. SiO_2, (f) Zr/Sm vs. SiO_2 variation diagrams for Pertek porphyries. HPFC: High-Pressure Fractional Crystallization involving garnet. Grt: garnet, Amp: amphibole (Zhang et al., 2014).

adakites (Figure 11a). Since all the Pertek adakitic samples overlap with the field of the slab-derived adakites, it can be inferred that they interacted with the mantle wedge during the upwelling of the melt (e.g., Defant and Kepezhinskas, 2001). These observations could be indicative of substantial interaction with the mantle in the genesis of Pertek adakites, which is also observed in the genesis of adakitic Saqqez-Takab pluton (Azizi et al., 2019).

In Figure 11b, the Th content of both oceanic arc- and continental margin-plutons (Kay et al., 2019) are compared. Pertek adakites, oceanic slab-derived adakitic granites (Kitakami Mts, Japan; Tsuchiya et al., 2005), postcollisional metasomatized mantle-derived Anatolian adakites (Ankara and Giresun, Şen and Şen, 2013; Yücel, 2018) and adakitic Saqqez-Takab pluton (Azizi et al., 2019) are plotted in this diagram. It is seen in the diagram that

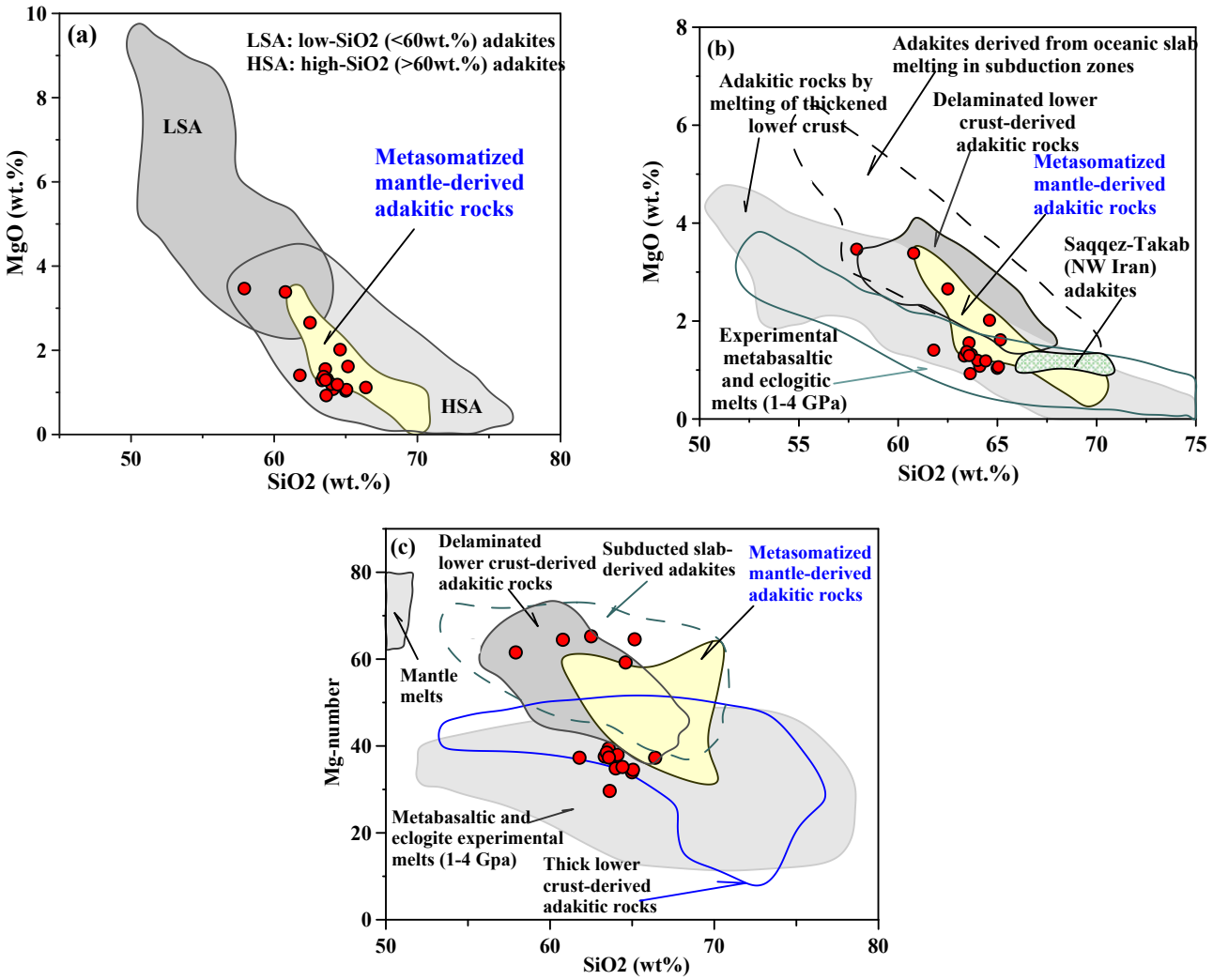

Figure 10. (a) MgO vs. SiO_2 diagram for Pertek andesitic-dacitic porphyries, Separation of high silica (HSA) and low silica (LSA) adakites adapted from Martin et al. (2005). (b) MgO vs. SiO_2 variation diagram (Wang et al., 2006) and (c) Mg# vs. SiO_2 variation diagram (Huang et al., 2013) for Pertek adakitic porphyries. Pertek samples show close affinity to metasomatized mantle-derived adakites from Iranian Azerbaijan (Lechmann et al., 2018) and crust-derived adakites. Data of Saqqez-Takab (NW Iran) adakites is from Azizi et al. (2019).

the Th contents of the Pertek adakitic samples are not only compatible with the continental plutons, but also show a tendency towards oceanic plutons. Compared to the oceanic slab-derived adakites of the subduction zone (e.g., adakitic granites from Kitakami area, Japan; Tsuchiya et al., 2005), the metasomatized mantle-derived adakitic rocks (e.g., Azizi et al., 2014; Lechmann et al., 2018), and lower crust-derived Malatya adakitic rhyolites, Pertek samples show a close similarity with the Iranian Azerbaijan and Saqqez-Takab samples, together with metasomatized mantle-derived Anatolian adakites (Figure 11b). Similar to the oceanic-slab-derived Kitakami adakitic granites, Hidden Bay Kagalaska oceanic granodiorites are characterized by low Th contents, in contrast to much higher contents of the Sierra continental granodiorites. However, the Pertek adakitic rocks overlap with continental arc plutons, and with those of metasomatized mantle-derived Iranian Azerbaijan and Anatolian adakites. Hence, we suggest that this reflects contributions of sources of (i) metasomatized mantle, which is modified by slab-derived fluids/melts and/or by sediment melts, and (ii) lower crust, to their genesis. Notably that a hybrid source is also suggested for the Dudurga (Sakarya, Central Pontide) adakitic intrusions (Çimen, 2020).

5.5. Sediment-melt and mantle interaction

To recognize the slab-derived agents, elemental ratios of REE and HFSE can be used. Because of their fractionation during melting of the slab, mantle-derived magmas

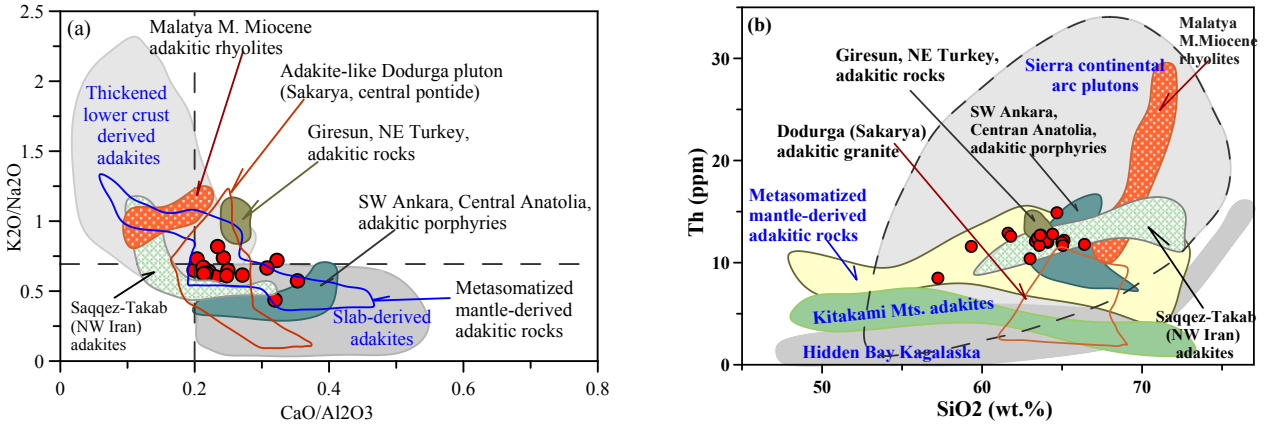

Figure 11. (a) K_2O/Na_2O vs. CaO/Al_2O_3 diagram for Pertek adakites (modified from Li et al., 2016), (b) Th vs. SiO_2 variation diagram shows comparison of Th concentrations of the Pertek adakitic rocks with those of the adakites in Sierra Nevada continental and Hidden Bay Kagalaska oceanic plutons (Kay et al., 2019). Slab melt/mantle derived Kitakami mounts adakite data are from Tsuchiya et al. (2005). Metasomatized mantle-derived adakitic volcanic rocks in Iranian Azerbaijan (Miocene-Quaternary) are adapted from Lechmann et al. (2018), Malatya adakitic rhyolites after Yılmaz et al. (2007). Ankara, Central Anatolia Miocene metasomatized mantle derived adakitic dacite samples from Şen and Şen (2013), Giresun adakitic porphyry samples from Yücel (2018), Saqqez-Takab (NW Iran) adakite samples are from Azizi et al. (2019). For comparison, data of adakite-like Dodurga (Sakarya, Central Pontide) pluton with hybrid origin (Çimen, 2020) are also plotted.

enriched by slab melts display elevated REE contents and enrichment in Nb/Zr and depletion in Th/Zr ratios (cf., e.g., Hawkesworth et al., 1997; Kepezhinskas et al., 1997; Liu and Zhao, 2019). The Pertek adakitic rocks have low Nb/Zr (0.05–0.07) and high Th/Zr (0.06–0.09) ratios, indicating that slab melts did not play an important role in their genesis (Figure 12a). Similarly, slab fluids are characterized by enrichment in LILEs and depletion in HFSE (Hawkesworth et al., 1997; Class et al., 2000). The Nb/Yb and Th/Yb ratios of the Pertek adakitic rocks indicate that, together with the metasomatized mantle-derived adakitic rocks, they have hybrid melt characteristics and their mantle source domain was infiltrated by slab fluids (Figure 12b). In contrast, subducted sediment melts increases the Th/Zr, Nb/Zr, and $La/Sm_{(N)}$ ratios of the mantle source (e.g., Nichols et al., 1994; Class et al., 2000). Similarly, subducted sediment melts rich in Th and LREE, whereas slab fluids contain elevated concentrations of Ba, Sr, U, and Pb (e.g., Hawkesworth et al., 1997; Guo et al., 2005, 2007; Zhu et al., 2009). In modern arc settings, subducted sediments show high Th/Yb ratios, in contrast to the fluid-dominated arcs with low Th/Yb ratios (< 1, Woodhead et al., 2001; Nebel et al., 2007). The Pertek adakitic rocks have Th/Yb ratios ranging from 17 to 28, suggesting a significant contribution from sediments in their origin. Accordingly, relative to Hf/Sm ratios of OIB (0.78), PM (0.70; Sun and McDonough, 1989) and MORB (0.78) (Sun and Mc-Donough, 1989) and GLOSS (0.70; Plank and Langmuir, 1998), the Hf/Sm ratios (0.8–1.23) of Pertek adakitic rocks are close to that of continental crust (CC) (0.68–1.13; Rudnick and Gao, 2003) and are comparable with those of metasomatized mantle-derived adakites (0.4–2.2, Lechmann et al., 2018).

In the primitive mantle-normalized multielement diagram, the large ion lithophile elements (LILE, e.g., Ba, Rb, and Th) of the Pertek adakites are slightly enriched, while some high field strength elements (HFSE, e.g., Nb, Ta, and Ti) are similar to slab-derived adakites and others (Figures 7a and 7b). They also show significant negative Nb-Ta and Ti anomalies. Overall samples demonstrate weak Eu anomalies ($Eu/Eu^* = 0.81–0.89$) (Figure 7b). Observed trace element compositions (see Figure 7a) (e.g., with depletion in Nb-Ta and Ti and high concentrations of LILE) can be attributed to metasomatized mantle wedges (Kheirkhah et al. 2009, 2013; Moghadam et al., 2014; Lechmannn et al., 2018). A refractory, mantle source contaminated by crust-derived sediment for western Anatolia K-rich magmas is also suggested by Çoban and Flower (2007), Helvacı et al. (2009) and Karaoğlu et al. (2010). Palmer et al. (2019) suggest that potassic volcanic rocks in Western Anatolia are characteristic of collisional tectonic zones, with recycling of continental crust playing an important role in their generation. Subduction-modified mantle metasomatism requires the slab melt- and sediment-melt-mantle interaction during oceanic slab subduction, but the melting of the metasomatized mantle is far from the subduction event in time (e.g., Guo et al., 2009). Based on these observations, the earlier sediment melt-mantle interaction processes possibly played a major role in the genesis of the Pertek adakitic volcanic rocks.

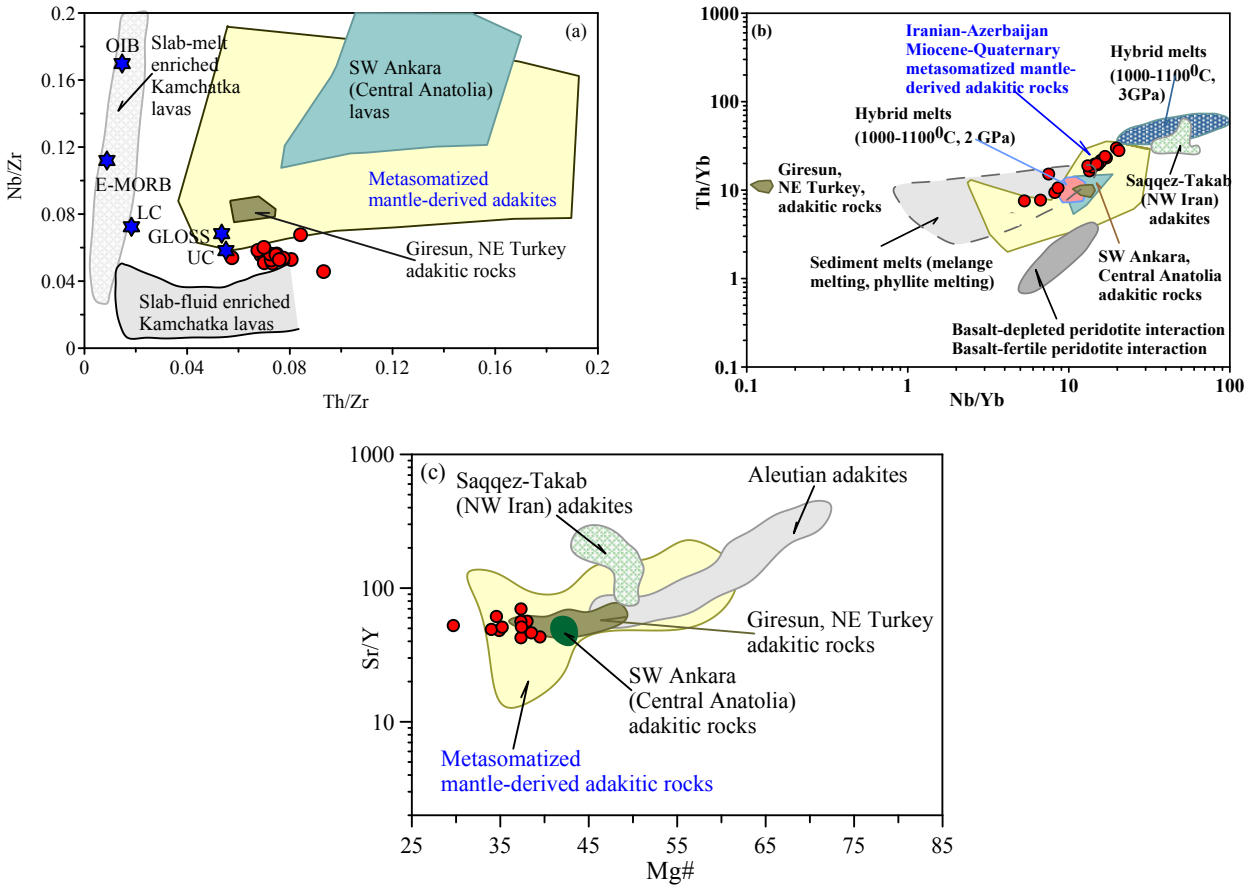

Figure 12. (a) Nb/Zr vs. Th/Zr diagram for Pertek adakitic volcanic rocks which differentiating subducted sedimentary related inputs. Fields of Kamchatka lavas are from Kepezhinskas et al. (1997) and Liu and Zhao (2019). (b) Variations of Th/Yb vs. Nb/Yb ratios of experimental melts compared to Pertek adakitic andesite-dacites with K_2O of 1.8–3.05 wt%. Note the difference between direct melts of sediment and hybrid melts. Data for basalt-depleted/fertile peridotite interaction, and sediment melts, and hybride melts from Wang and Foley (2018, references therein). Adakitic porphyries from Giresun (NE Turkey) (Yücel, 2018) and Ankara (Central Anatolia) (Şen and Şen, 2013) are also plotted for comparison. Saqqez-Takab (NW Iran) adakitic pluton (Azizi et al., 2019). (c) Sr/Y vs. Mg# plots of Aleutian and Pertek adakitic volcanics in diagram. Aleutian adakite samples are from Yogodzinski et al. (2001).

In this regard, the formation of metasomatism in the lithospheric mantle can be explained by hybrid melts from crust-derived sediments and oceanic peridotitic crust, which react with wall-rock peridotite to form metasomatic domains in the mantle.

For the interaction between the ultradepleted peridotite and continental crust-derived sediment, and overlying mantle wedge reacting to produce hybrid magmas, and formation of the metasomatized mantle, a series of high-pressure interaction experiments have been performed (Wang et al., 2017; Wang and Foley, 2018) between phyllitic metasediment and a depleted peridotite (dunite) at 2–3 GPa. The high Th/Yb versus Nb/Yb ratios seen in Pertek adakitic rocks indicate such a hybridization (Figure 12b). The Pertek samples plot well within the array between 2 GPa and 3 GPa experimental hybrid melts and show a positive trend, which is also consistent with those of Iran-Azerbaijan metasomatized mantle-derived adakitic rocks and Iran Saqqez-Takab adakitic pluton. In this diagram, both Th/Yb and Nb/Yb fractionations increase with increasing pressure. This observation is consistent with a hybrid origin for Pertek adakitic rocks.

Melting conditions of the magma that produced the Pertek adakitic porphyries also show that they differ from the adakites in Aleutian island arcs (in the northernmost part of the circum Pacific, the west to Alaska) (Yogodzinski et al., 2001) that are one of the best examples of subduction-related slab-derived adakites, in the Sr/Y vs. Mg# diagram (Figure 12c).

6. Geodynamic interpretation

Recent mantle tomographical studies (Barazangi et al., 2006; Skobeltsyn et al., 2014; Kaban et al., 2018; Portner et al., 2018) revealed that subduction of the Neo-Tethys

lithosphere occurred before the initiation of the continent-continent collision of Arabia and Eurasia. Regional uplift commenced at approximately 20 Ma in the east and propagated west in the region (McNab et al., 2018). The timing of the initiation of continental collision between the Arabian and Eurasian plates is still debated. Contrary to the view of Early to Middle Miocene (Okay et al., 2010; Karadenizli et al., 2016; Açlan and Altun, 2018; Gülyüz et al., 2020) and Middle Miocene periods (Cavazza et al., 2018) for the onset of collision, van Hunen and Allen (2011), McQuarrie and van Hinsbergen (2013) and Koshnaw et al. (2017) advocated that by Middle Oligocene (approximately 26–27 Ma), Neo-Tethys oceanic crust had been consumed, and the Arabia-Eurasia continent-continent collision initiated. On the other hand, for the Caucasus-Iran-Anatolia (CIA) collisional zone volcanism, Lin et al. (2020) proposed a double subduction scenario (e.g., Skobeltsyn et al., 2014) and double slab break-off model (Erzurum-Kars Suture Zone in Pontide at North, Bitlis-Zagros Suture Zone in SE Anatolia at South), and suggested that break-off events occurred at ≈ 17 Ma (Early Miocene) at South (Bitlis-Zagros Suture Zone) and ≈ 9 Ma at North (Erzurum-Kars Suture Zone). The authors indicated that an early slab break-off at approximately 7 Ma along the Bitlis-Zagros Suture is supported by apatite fission-track age data that suggest rapid exhumation in the Bitlis thrust zone between 18 and 13 Ma (Okay et al., 2010). The slab-like high-velocity anomalies beneath the EAAC, Pontides, and the Caucasus are interpreted as the detached southern and northern Neo-Tethys slabs (Zor 2008). Indeed, break-off of the Bitlis slab has been estimated to have occurred during the middle to late Miocene based on the timing of magmatic events (e.g., Şengör et al., 2008; Çolakoğlu and Arehart, 2010; Ekici, 2016; Racano et al., 2021), against to Oligocene suggested by Kounoudis et al., (2020), and seismic and mantle tomographic images (slab-like high-velocity anomalies) also show that slab fragments now reside within or below the mantle transition zone (e.g., Zor et al., 2008; Portner et al., 2018; Reid et al., 2019).

On the genesis of Elazığ-Tunceli Neogene volcanism, Agostini et al. (2019) and Di Giuseppe et al. (2021) envisaged that the Early-Middle Miocene magmas, emplaced in a convergent setting (active subduction), indicate derivation from mantle sources modified by subduction components. In contrast, we propose here that the magmatic output of the Pertek (Tunceli) adakitic rocks was not temporospatial associated with active subduction and slab-derived melts. Active subduction continued to Early Miocene time concurrently with Arabian-Anatolian soft collision. During this period, the Bitlis slab and continental subduction (e.g., McQuarrie and van Hinsbergen, 2013; Kaban et al., 2018) modified the mantle wedge via slab- and continent-derived sediment melts. As discussed before, the adakitic rocks found in NW Iran, which are the geotectonic continuation of eastern Anatolia (e.g., Azizi et al., 2014, 2019, 2021 and Lechmann et al., 2018) show geochemical similarities with the Pertek adakites. Azizi et al. (2021) suggested that Early Miocene adakitic andesites (18–15 Ma) in the NW Iran area were generated after collision (postcollisional), which was also associated with doubling of the thickness of the continental crust in the Zagros suture zone, thinning of continental crust far from the Zagros suture zone, and development of shallow-basin sedimentary rocks in NW Iran. Similarly, Topuz et al. (2019) suggested that the Early Miocene represents probably a time of continental extension and exhumation in Eastern Anatolia and NW Iran. However, recent studies (e.g., Karadenizli et al., 2016; Gülyüz et al., 2020) confirm the Miocene time of collision between Eurasian and Arabian plates, which are also consistent with the proposed model of Okay et al. (2010) and Cavazza et al. (2018). Based on anisotropy data of magnetic susceptibility of the dated sedimentary sequences from East Anatolia, Gülyüz et al. (2020) contend that the Early to Middle Miocene period marks the onset of continental (hard) collision between Eurasia and Arabia and the initiation of collision-related uplift in the region. Similarly, Karadenizli et al. (2016) suggested the end of Early Miocene time for the collision of Arabian and Anatolian plates, based on the basin analysis of Central Eastern Anatolia. In this regard, a significant crustal thickening in the region during the Early to Middle Miocene magmatism can be expected, and infer from using La/Yb ratios (e.g., Kay and Kay, 2002). Plotting La/Yb ratios versus ages of these adakitic porphyries and Late Oligocene rhyolites (Figure 13) suggests the former to have been generated with a much thicker crust. In the plot (Figure 13), there are large ranges in La/Yb ratios and thus the hypothesized crustal thickness during the collisional Early to Miocene period. Based on these observations, we concluded that the Eastern Anatolian Neogene volcanism was driven by active asthenospheric mantle (e.g., Çoban, 2007), and was linked to the collision between Arabian and Eurasian plates and the associated break-off of the Bitlis slab. Hence, asthenospheric mantle flows and the uplift-related lithospheric tectonics (e.g., Karaoğlu et al., 2017) triggered the partial meltings in the mantle lithosphere and associated lower crustal sources in the region. The collision-related uplift and extension-related volcanism must have dominated all over the region.

Considering the regional magmatic activities, geochemical signatures of Pertek adakitic porphyries are analogous to metasomatized mantle-derived adakitic porphyries especially Iranian-Azerbaijan (Lechmann et al., 2018) and Anatolian examples (e.g., SW Ankara,

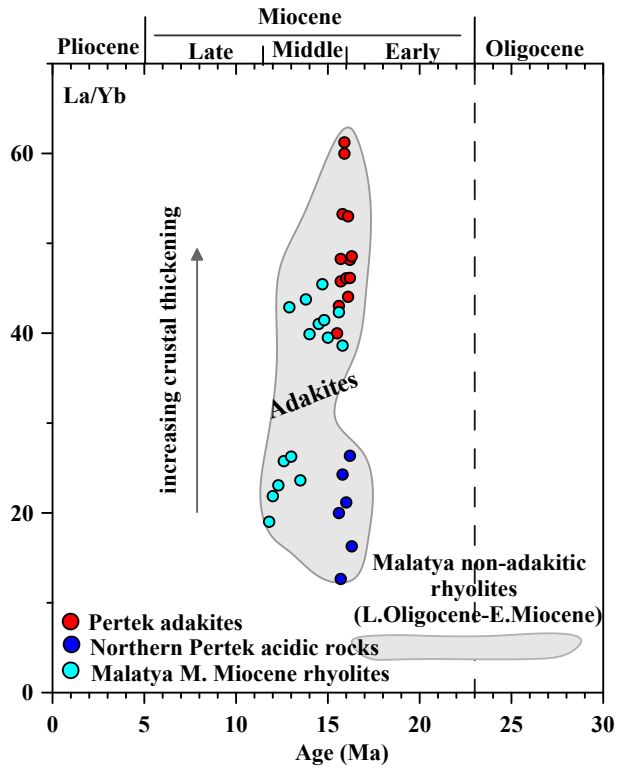

Figure 13. Plots of La/Yb ratios vs. magmatic ages for the Pertek adakitic porphyries and Malatya and in the North of Pertek adakitic volcanics - Malatya nonadakitic rhyolites. The increasing crustal thickness is from Kay and Kay (2002). Dramatic increase in La/Yb ratios of the rocks corresponds to hard continental collision and crustal thickening. Northern Pertek acidic rocks from Di Giuseppe et al. (2017), Malatya middle Miocene rhyolites and non adakitic rhyolites from Yılmaz et al. (2007).

Central Anatolia, Şen and Şen, 2013; Giresun, NE Turkey, Yücel, 2018), rather than slab-derived modern adakites (e.g., Aleutians). The collision-related (or postcollisional) volcanic activities in the region (Figures 1a–1e and 2) produced basaltic to rhyolitic lavas and pyroclastic rocks (Pearce et al., 1990; Keskin et al., 1998; Yılmaz et al., 1998). The study area forms the westernmost part of the calc-alkaline volcanic province with the same age (16.2–15.7 Ma) in the near vicinity (Di Giuseppe et al., 2017). In the southern part of the study area, the Late Oligocene to Early Miocene Malatya nonadakitic rhyolites represent the earliest phases of volcanic activity in the region whereas the Middle Miocene Malatya felsic-rhyolites (adakitic) represent typical lower crust-derived melts (Yılmaz et al., 2007). On the other hand, in the northern part of the study area, geochemical data of Early-Middle Miocene Pertek adakite-like andesites and acidic volcanic rocks indicate the role of predominantly metasomatized lithospheric mantle-derived melts in the region (e.g., Di Giuseppe et al., 2017). Accordingly, the geochemical signatures of southern Pertek rocks are also consistent with a lower crustal origin. Hence, we proposed a hybrid origin for the Pertek adakitic rocks. A mixture of melts fed by sources from both amphibolitic lower crust and metasomatized subcontinental lithospheric mantle is the most likely parental magma to the Pertek adakitic porphyries. It is also clear in Figures 10–12 that the volcanic rocks cropping out in the region and surroundings have not been defined as adakitic in nature in previous studies (Yılmaz et al., 2007; Ekici, 2016; Di Giuseppe et al., 2017). Thus, the adakitic volcanism in the region is not a local petrological event but has regional importance and indicates the shifting geotectonic regime that caused the initiation and formation of slab break-off-related Neogene adakitic melt in Eastern Anatolian Volcanic Province, concurrently or later Early to Miocene hard collision of Arabian and Anatolian plates. Accordingly, Neogene basaltic volcanism initiated at 17 Ma in the Arabian foreland (Karacadağ volcanism, Ekici and Macpherson, 2019) and the onset of the Arabian foreland at 17.6 Ma (Yamadağ and Arapkir volcanism, Kürüm et al., 2008), nearly coeval with the regional uplift due to the collision, slab break-off (e.g., Hunen and Allen, 2011; Bottrill et al., 2012) and mantle upwelling.

7. Concluding remarks

In this study, we focused on the andesitic-dacitic volcanic association cropping out in the Pertek area (to the north of Elazığ and southwest of Tunceli) from Eastern Anatolia postsubductional setting. The results obtained from the geochemical characteristics of these intermediate-acidic volcanic rocks are summarized below.

High-K, calc-alkaline andesite-dacites in Pertek areas show an adakitic character with their high Sr/Y, La/Yb, and low Y contents. These adakitic rocks, defined as high-silica adakites, have some characteristics of both oceanic and continental adakites. Based on their geochemical signatures, it is suggested that the Pertek adakitic volcanic rocks originated from a hybrid source. The parental magma from which Pertek adakitic rocks were originated, was formed by the mixture of melts, derived from sources of both metasomatized peridotitic mantle and lower crust. Considering the geotectonic regime in the region, it is concluded that, the subduction and closure of Neotethys Ocean, and pre-Early Miocene arc-continent and continent-continent soft collisions and continental subduction modified the mantle wedge beneath Eastern Anatolian. Early to the Middle Miocene hard collision between Arabia and Eurasia plates caused the break-off of the Bitlis slab (collision-induced slab break-off). Hence, collision- and break-off-induced asthenospheric mantle upwelling, and ongoing regional uplifting, and related tectonics triggered the partial melting of metasomatized

lithospheric mantle. Lithospheric mantle-derived magmas also caused by contemporaneous melting in the lower crust, which became thicker due to the continental collision, and finally, the mixture of varying amounts of these melts produced the Pertek adakitic magmas similar to the formation of other adakitic rocks in East Anatolia (postsubductional) collisional-related tectonic setting.

Acknowledgments
This study was funded by the Scientific Research Projects Unit (FÜBAP, Project number: MF-13. 09) of Fırat University (Elazığ, Turkey). We thank Okay Çimen, Özgür Karaoğlu and Hossein Azizi for their very constructive comments and recommendations, which led to significant improvement of the paper.

References

Açlan M, Altun Y (2018). Syn-collisional I-type Esenköy Pluton (Eastern Anatolia-Turkey): an indication for collision between Arabian and Eurasian plates. Journal of African Earth Sciences 142: 1–11.

Agostini S, Doglioni C, Innocenti F, Manetti P, Tonarini S et al. (2007). The transition from orogenic to intraplate Neogene magmatism in Western Anatolia and Aegean area. In: Beccaluva L, Bianchini G, Wilson M (editors). Cenozoic Volcanism in the Mediterranean Area. Geological Society of American Special Paper 418: 1–15.

Agostini S, Doglioni C, Innocenti F, Manetti P, Tonarini S (2010). On the geodynamics of the Aegean rift. Tectonophysics 488: 7–21.

Agostini S, Savaşçın MY, Di Giuseppe P, Di Stefano F, Karaoğlu Ö et al. (2019). Neogene volcanism in Elazığ-Tunceli area (eastern Anatolia): geochronological and petrological constraints. Italian Journal of Geosciences 138: 435-455.

Aksoy E, Türkmen İ, Turan M (2005). Tectonics and sedimentation in convergent margin basins: an example from the Tertiary Elazığ basin, Eastern Turkey. Journal of Asian Earth Sciences 25: 459–472.

Aktağ A, Öztüfekçi Önal A, Sayit K (2019). Geochemistry of the post-collisional Miocene mafic Tunceli Volcanics, Eastern Turkey: Implications for the nature of the mantle source and melting systematics. Geochemistry 79: 113-129.

Alonso-Perez R, Müntener O, Ulmer P (2009). Igneous garnet and amphibole fractionation in the roots of island arcs: experimental constraints on andesitic liquids. Contributions to Mineralogy and Petrology 157: 541–558.

Anders E, Grevesse N (1989). Abundances of the elements: meteoric and solar. Geochimica et Cosmochimica Acta 53: 197-214.

Atherton MP, Petford N (1993). Generation of sodium-rich magmas from the newly underplated basaltic crust. Nature 362: 144–146.

Azizi H, Asahara Y, Tsuboi M, Takemura K, Razyani S (2014). The role of the heterogenetic mantle in the genesis of adakites northeast of Sanandaj, northwestern Iran. Geochemistry 74 (1): 87-97.

Azizi H, Stern R, Topuz G, Asahara Y, Moghadam HS (2019). Late Paleocene adakitic granitoid from NW Iran and comparison with adakites in the NE Turkey: Adakitic melt generation in the normal continental crust. Lithos 346 (347): 105151.

Azizi H, Daneshvar N, Mohammadi A, Asahara Y, Whattam SA et al. (2021). Early Miocene post-collision andesite in the Takab area, northwest Iran. Journal of Petrology, egab022. doi: 10.1093/petrology/egab022

Barazangi M (1989). Continental collision zones: Seismotectonics and crustal structure. In: James DE (editor). The encyclopedia of solid earth geophysics: Van Nostrand Reinhold Company, New York, pp. 58-75.

Bernard A, Demaiffe D, Mattielli N, Punongbayan RS (1991). Anhydrite-bearing pumices from Mount Pinatubo: further evidence for the existence of sulfur-rich silicic magmas. Nature 354: 139–140.

Bernard A, Knittel U, Weber B, Weis D, Albrecht A et al. (1996). Petrology and geochemistry of the 1991 eruption products of Mount Pinatubo (Luzon, Philippines). In: Newhall CG and Punongbayan RS (editors). Fire and Mud. Eruptions and Lahars of Mount Pinatubo, Philippines. Seattle: University of Washington Press, pp. 767–798.

Bottrill AD, Van Hunen J, Allen MB (2012). Insight into collision zone dynamics from topography: numerical modelling results and observations. Solid Earth 3: 387-399.

Bullen TD, Clynne MA (1990). Trace element and isotopic constraints on magmatic evolution at Lassen volcanic center. Journal of Geophysical Research 95: 19671–19691.

Castillo RP (2006). An overview of adakite petrogenesis. Chinese Science Bulletin 51: 257–268.

Castillo PR (2012). Adakite petrogenesis. Lithos 13: 304-316.

Castillo PR, Janney PE, Solidum RU (1999). Petrology and geochemistry of Camiguin Island, southern Philippines: insights to the source of adakites and other lavas in a complex arc setting. Contributions to Mineralogy and Petrology 134: 33-51.

Cavazza W, Cattò S, Zattin M, Okay AI, Reiners P (2018). Thermochronology of the Miocene Arabia-Eurasia collision zone of southeastern Turkey: Geosphere 14: 2277–2293.

Class C, Miller DM, Goldstein SL, Langmuir CH (2000). Distinguishing melt and fluid subduction components in Umnak Volcanics, Aleutian Arc. Geochem Geophys Geosyst 1999GC000010.

Chung SL, Liu D, Ji J, Chu MF, Lee HY et al. (2003). Adakites from continental collision zones: melting of the thickened lower crust beneath southern Tibet. Geology 31: 1021–1024.

Çimen O (2020). Geochemical characteristics of the adakite-like Dodurga Pluton (Central Pontides, N Turkey): Implications for Middle Triassic continental arc magmatism in southern Black Sea region. International Journal of Earth Sciences (Geologische Rundschau) 109: 809–829.

Çoban H (2007). Basalt magma genesis and fractionation in collision-and extension-related provinces: a comparison between eastern, central and western Anatolia. Earth-Science Reviews 80: 219-238.

Çoban H, Caran Ş, Kumral M, Karslı O, İmamoğlu Ş (2007). Adakite-like, A-type and OIB-like magmas from Anatolia-Arabian post-collisional settings. Asia Oceania Geosciences Society 4. Annual Meeting, Bangkok. 253.

Çoban H, Karslı O, Caran Ş, Yılmaz K (2020). Sediment-derived melt-related metasomatized mantle wedge as a source of post-subduction Quaternary adakitic porphyries associated with absarokite-shoshonite from the Karadağ stratovolcano (Karaman, Central Anatolia, Turkey). Journal of Asian Earth Sciences 196-1.

Çolakoğlu A R, Arehart GB (2010). The petrogenesis of Sarıcimen (Caldıran-Van) quartz monzodiorite: Implication for initiation of magmatism (late Medial Miocene) in the east Anatolian collision zone, Turkey. Lithos 119 (3): 607–620.

Defant M J, Drummond MS (1990). Derivation of some modern arc magmas by melting of young subducted lithosphere. Nature 347: 662-665.

Defant M, Kepezhinskas P (2001). Evidence suggests slab melting in arc magmas. Eos Transactions American Geophysical Union 82: 67-70.

Deng C, Sun G, Sun D, Huang H, Zhang J et al. (2018). Origin of C type adakite magmas in the NE Xing'an block, NE China and tectonic implication. Acta Geochimica 37: 281–294.

Di Giuseppe P, Agostini S, Lustrino M, Karaoğlu Ö, Savaşçın MY et al. (2017). Transition from compression to strike-slip tectonics revealed by Miocene-Pleistocene volcanism west of the Karlıova Triple Junction (East Anatolia). Journal of Petrology 58 (10): 2055-2087.

Di Giuseppe P, Agostini S, Di Vincenzo G, Manetti P, Savaşçın MY et al. (2021). From subduction to strike slip-related volcanism: insights from Sr, Nd, and Pb isotopes and geochronology of lavas from Sivas–Malatya region, Central Eastern Anatolia. International Journal of Earth Sciences 110: 849–874. doi: 10.1007/s00531-021-01995-0

Doglioni C, Agostini S, Crespi M, Innocenti F, Manetti P et al. (2002). On the extension in western Anatolia and the Aegean sea. Journal of the Virtual Explorer 8: 169-184.

Ekici T, Alpaslan M, Parlak O, Ucurum A (2009). Geochemistry of the Middle Miocene collision-related Yamadağı (Eastern Anatolia) calc-alkaline volcanics, Turkey. Turkish Journal of Earth Sciences 18: 511–528.

Ekici T (2016). Collision-related slab break-off volcanism in the Eastern Anatolia, Kepez volcanic complex (Turkey). Geodinamica Acta 28 (3): 223-239.

Ekici T, Macpherson CG (2019). Convergence-aligned foreland magmatism in the Arabia-Anatolia Collision: geochronological evidence from the Karacadağ Volcanic Complex, south-east Turkey. Turkish Journal of Earth Sciences 28: 719-733

Eyüboğlu Y, Santosh M, Chung SL (2011a). Crystal fractionation of adakitic magmas in the crust–mantle transition zone: petrology, geochemistry, and U–Pb zircon chronology of the Seme adakites, eastern Pontides, NE Turkey. Lithos 121: 151–166.

Eyüboğlu Y, Santosh M, Chung SL (2011b). Petrochemistry and U-Pb zircon ages of adakitic intrusions from the Pulur Massif (Eastern Pontides, NE Turkey): Implications for slab rollback and ridge subduction associated with Cenozoic convergent tectonics in the Eastern Mediterranean. Journal of Geology 119: 394–417.

Eyüboğlu Y, Chung S, Santosh M, Dudas FO, Akaryalı E (2011c). Transition from shoshonitic to adakitic magmatism in the eastern Pontides, NE Turkey: Implications for slab window melting. Gondwana Research 19 (2): 413-429.

Eyüboğlu Y, Santosh M, Yi K, Bektaş O, Kwon S (2012). Discovery of Miocene adakitic dacite from the Eastern Pontides Belt and revised geodynamic model for the late Cenozoic Evolution of the eastern Mediterranean region. Lithos 146 (147): 218-232.

Göncüoğlu MC (2010). Introduction to the geology of Turkey: Geodynamıc evolution of the pre-Alpine and Alpine terranes. Middle East Technical University pp. 69.

Guidotti CV (1984). Micas in metamorphic rocks. In: Bailey SW (ed.) Micas. Reviews in Mineralogy, Mineralogical Society of America 13: 357–468.

Guo JH, Chen FK, Zhang XM, Siebel W, Zhai MG (2005). Evolution of syn-to post-collisional magmatism from north Sulu UHP belt, eastern China: zircon U–Pb geochronology. Acta Petrologica Sinica 4: 1281–1301 (in Chinese with English abstract).

Guo Z, Wilson M, Liu J (2007). Post-collisional adakites in south Tibet: Products of partial melting of the subduction-modified lower crust. Lithos 96: 205–224.

Guo F, Fan W, Li C, Gao X, Miao L (2009). Early Cretaceous highly positive -Nd felsic volcanic rocks from the Hinggan mountains, NE China: origin and implications for Phanerozoic crustal growth. International Journal of Earth Science 98: 1395–1411.

Gülen L (1984). Sr, Nd, Pd isotope and trace elements geochemistry of calc-alkaline and alkaline volcanics, eastern Turkey. Ph.D. Massachusetts Institute of Technology, Cambridge.

Gülyüz E, Durak H, Özkaptan M, Krijgsman W (2020). Paleomagnetic constraints on the early Miocene closure of the southern Neo-Tethys (Van region; East Anatolia): Inferences for the timing of Eurasia-Arabia collision. Global and Planetary Change 185: 103089.

Hawkesworth CJ, Turner SP, McDermott F, Peate DW, Van Calsteren P (1997). U-Th isotopes in arc magmas: Implications for element transfer from the subducted crust, Science 276: 551–555.

Hawthorne FC (1983). The crystal chemistry of the amphiboles. Canadian Mineralogist 21: 173-480.

Helvacı C, Ersoy Y, Sözbilir H, Erkül F, Sümer Ö et al. (2009). Geochemistry and 40Ar/39Ar geochronology of Miocene volcanic rocks from the Karaburun Peninsula: Implications for amphibole-bearing lithospheric mantle source, Western Anatolia. Journal of Volcanology and Geothermal Research 185: 181-202.

Herece Eİ, Acar Ş (2016). Upper Cretaceous-Tertiary geology and stratigraphy of Pertek and its vicinity (Tunceli, Turkey). Bulletin of the Mineral Research and Exploration 153: 1-44.

Huang F, Chen L, Wu Z, Wang W (2013). First-principles calculations of equilibrium Mg isotope fractionations between garnet, clinopyroxene, orthopyroxene, and olivine: Implications for Mg isotope thermometry. Earth and Planetary Science Letters 367: 61–70.

Innocenti F, Mazzuoli R, Pasquare G, Radicati Di Brozolo F et al. (1976). Evolution of the volcanism in the area of interaction between the Arabian, Anatolian and Iranian plates (lake Van, Eastern Turkey). Journal of Volcanology Geothermal Research 1: 103-112.

Innocenti F, Mazzuoli R, Pasquar G, Radicati Di Brozolo F et al. (1982). Tertiary and Quaternary volcanism of the Erzurum-Kars area (Eastern Turkey): Geochronological data and geodynamic evolution. Journal of Volcanology Geothermal Research 13: 223-240.

Innocenti F, Agostini S, Di Vincenzo G, Doglioni C, Manetti P et al. (2005). Neogene and Quaternary volcanism in Western Anatolia: Magma sources and geodynamic evolution. Marine Geology 221: 397-421.

Kaban MK, Petrunin AG, El Khrepy S, Al-Arifi N (2018). Diverse continental subduction scenarios along the Arabia-Eurasiacollision zone. Geophysical Research Letters 45: 6898–6906.

Kadıoğlu YK, Dilek Y (2010). Structure and geochemistry of the adakitic Horoz granitoid, Bolkar Mountains, south-central Turkey, and its tectonomagmatic evolution. International Geology Review 52: 505–535.

Kamvong T, Meffre S, Maas R, Stein H, Lai CK (2014). Adakites in the Truong Son and Loei fold belts, Thailand and Laos: genesis and implications for geodynamics and metallogeny. Gondwana Research 26: 165–184.

Karadenizli L, Varol BE, Saraç G, Gedik F (2016). Late eocene-early miocene palaeogeographic evolution of central Eastern Anatolian basins, the closure of the neo-tethys ocean and continental collision. Journal Geological Society of India 88: 773-798.

Karaoğlu Ö, Helvacı C, Ersoy Y (2010). Petrogenesis and $^{40}Ar/^{39}Ar$ geochronology of the volcanic rocks of the Uşak-Güre basin, western Türkiye. Lithos 119/3–4: 193–210.

Karaoğlu Ö, Selçuk AS, Gudmundsson A (2017). Tectonic controls on the Karlıova triple junction (Turkey): Implications for tectonic inversion and the initiation of volcanism. Tectonophysics 694: 368-384.

Karaoğlu Ö, Gülmez F, Göçmengil G, Lustrino M, Di Giuseppe P et al. (2020). Petrological evolution of Karlıova-Varto volcanism (Eastern Turkey): Magma genesis in a transtensional triple-junction tectonic setting. Lithos 364–365: 1-15.

Karslı O, Dokuz A, Uysal İ, Aydın F, Kandemir R et al. (2009). Generation of the Early Cenozoic Adakitic Volcanism by Partial Melting of Mafic Lower Crust, NE Turkey: Implications for Crustal Thickening to Delamination. II. International Symposium on the Geology of the Black Sea Region, Ankara, Türkiye. pp. 99-100.

Karslı O, Dokuz A, Uysal İ, Aydın F, Kandemir R et al. (2010). Generation of the Early Cenozoic adakitic volcanism by partial melting of the mafic lower crust, Eastern Turkey: implications for crustal thickening to delamination. Lithos 114: 109–120.

Karslı O, Uysal İ, Ketenci M, Dokuz A, Kandemir R et al. (2011). Adakite-like granitoid porphyries in Eastern Turkey: potential parental melts and geodynamic implications. Lithos 127: 354-372.

Karslı O, Uysal İ, Dilek Y, Aydın F, Kandemir R (2013). Geochemical modeling of early Eocene adakitic magmatism in the Eastern Pontides, NE Anatolia: continental crust or subducted oceanic slab origin? International Geology Review 55 (16): 2083-2095.

Karslı O, Dokuz A, Kandemir R, Aydin F, Schmitt AK et al. (2019). Adakitic parental melt generation by partial fusion of the juvenile lower crust, Sakarya Zone, NE Turkey: A far-field response to break-off of the southern Neotethyan oceanic lithosphere. Lithos 338-339: 58-72.

Karslı O, Caran Ş, Çoban H, Şengün F, Tekkanat O et al. (2020). Melting of the juvenile lower crust in a far-field response to roll-back of the southern Neotethyan oceanic lithosphere: The Oligocene adakitic dacites, NE Turkey. Lithos 370-371: 105695.

Kay RW, Kay SM (2002). Andean adakites: three ways to make them. Acta Petrologica Sinica 18 (3): 303-311.

Kay SM, Ramos VA, Marquez M (1993). Evidence in Cerro Pampa volcanic rocks for slab-melting prior to ridge-trench collision in southern South America. Journal of Petrology 101: 703-714.

Kay SM, Jicha BR, Citron GL, Kay RW, Tibbetts AK et al. (2019). The Calc-alkaline Hidden Bay and Kagalaska Plutons and the construction of the Central Aleutian oceanic arc crust. Journal of Petrology 60 (2): 393–439.

Kepezhinskas P, McDermott F, Defant MJ, Hochstaedter A, Drummond MS et al. (1997). Trace element and Sr–Nd–Pb isotopic constraints on a three-component model of Kamchatka Arc petrogenesis: Geochimica et Cosmochimica Acta 3: 577–600.

Keskin M (2003). Magma generation by slab steepening and breakoff beneath a subduction accretion complex: an alternative model for collision-related volcanism in eastern Anatolia. Geophysical Research Letters 30: 8046-8050.

Keskin M (2005). Domal uplift and volcanism in a collision zone without a mantle plume: Evidence from Eastern Anatolia. http://www.mantleplumes. org/Anatolia.html.

Keskin M, Pearce JA, Mitchell JG (1998). Volcano-stratigraphy and geochemistry of collision-related volcanism on the Erzurum–Kars Plateau, northeastern Turkey. Journal of Volcanology Geothermal Research 85: 355–404.

Kheirkhah M, Allen MB, Emami M (2009). Quaternary syn-collision magmatism from the Iran/Turkey borderlands. Journal of Volcanology and Geothermal Research 182: 1–12.

Kheirkhah M, Neill I, Allen MB, Ajdari K (2013). Small-volume melts of lithospheric mantle during continental collision: Late Cenozoic lavas of Mahabad, NW Iran. Journal of Asian Earth Sciences 74: 37–49.

Koshnaw RI, Horton BK, Stockli DF, Barber DE, Tamar-Agha MY et al. (2017). Neogene shortening and exhumation of the Zagros fold-thrust belt and foreland basin in the Kurdistan region of northern Iraq. Tectonophysics 694: 332–355.

Kounoudis R, Bastow ID, Ogden CS, Goes S, Jenkins J et al. (2020). Seismic tomographic imaging of the Eastern Mediterranean mantle: Implications for Terminal-stage subduction, the uplift of Anatolia, and the development of the North Anatolian Fault. Geochemistry, Geophysics, Geosystems 21: e2020GC009009. doi: 10.1029/2020GC009009

Kürüm S, Akgül B, Erdem E (2006). Examples of neogene volcanism in Eastern Turkey: comparative petrographic, geochemical and petrologic features of Malatya-Elazığ-Tunceli volcanics. Journal of Geochemical Society of India 68: 129-136.

Kürüm S, Önal A, Boztuğ D, Spell T, Arslan M (2008). 40Ar/39Ar age and geochemistry of the post-collisional Miocene Yamadağvolcanics in the Arapkir area (Malatya Province), eastern Anatolia, Turkey. Journal of Asian Earth Sciences 33 (3-4): 229–251

Kürüm S, Akgül B, Önal AÖ, Boztuğ D, Harlavan Y et al. (2011). An example for arc-type granitoids along collisional zones: the Pertek granitoid, Taurus orogenic belt, Turkey. International Journal of Geosciences 2: 214-226.

Leake EB (1971). On aluminous and edenitic hornblendes. Mineralogical Magazine 38: 389-407.

Leake EB, Wooley AR, Arps CES, Birch WD, Gilbert MC et al. (1997). Nomenclature of amphiboles report of the subcommittee on amphiboles of the International Mineralogical Association Commission on New Minerals and Mineral Names. European Journal of Mineralogy 9: 623-651.

Lechmann A, Burg JP, Ulmer P, Guillong M, Faridi M (2018). Metasomatized mantle as the source of Mid-Miocene-Quaternary volcanism in NW-Iranian Azerbaijan: Geochronological and geochemical evidence. Lithos 304 (307): 311–328.

Le Maitre RW, Streckeisen A, Zanettin B, Le Bas MJ, Bonin B et al. (2002). Igneous Rocks: A classification and glossary of terms, recommendations of the international union of geological sciences, subcommission of the systematics of igneous rocks. Cambridge University Press, Cambridge, UK. London, Special Publications 16: 59-76.

Li SM, Zhu DC, Wang Q, Zhao Z, Zhang LL et al. (2016). Slab-derived adakites and subslab asthenosphere-derived OIB-type rocks at 156 ± 2 Ma from the north of Gerze, central Tibet: Records of the Bangong–Nujiang oceanic ridge subduction during the Late Jurassic. Lithos 262: 456–469.

Lin YC, Chung S, Bingöl AF, Yang L, Okrostsvaridze A et al. (2020). Diachronous initiation of post-collisional magmatism in the Arabia-Eurasia collision zone. Lithos 356 (357): 1-15.

Liu H, Zhao JH (2019). Slab breakoff beneath the northern Yangtze Block: Implications from the Neoproterozoic Dahongshan mafic intrusions. Lıthos https://doi.org/10.1016/j.lithos.2019.05.037

Liu S, Hu RZ, Feng CX, Zhou HB, Li C et al. (2008). Cenozoic high Sr/Y volcanic rocks in the Qiangtang terrane, northern Tibet: geochemical and isotopic evidence for the origin of delaminated lower continental melts. Geological Magazine 145: 463–474.

Ma L, Wang BD, Jiang ZQ, Wang Q, Li ZX et al. (2012). Petrogenesis of the Early Eocene adakitic rocks in the Napuri area, southern Lhasa: Partial melting of the thickened lower crust during slab break-off and implications for crustal thickening in southern Tibet. Lithos 196–197: 321–338.

Macpherson CG, Dreher ST, Thirlwall MF (2006). Adakites without slab melting: high-pressure differentiation of island arc magma, Mindanao, the Philippines. Earth and Planetary Science Letters 243: 581-593.

McNab F, Ball PW, Hoggard MJ, White NJ (2018). Neogene uplift and magmatism of Anatolia: Insights from drainage analysis and basaltic geochemistry. Geochemistry, Geophysics, Geosystems 19 (1): 175–213.

Martin H (1999). Adakitic magmas: modern analogues of Archaean granitoids. Lithos 46: 411-429.

Martin H, Smithies RH, Rapp R, Moyen JF, Champion D (2005). An overview of adakite, tonalite-trondhjemite-granodiorite (TTG), and sanukitoid: relationships and some implications for crustal evolution. Lithos 79: 1-24.

McQuarrie N, Van Hinsbergen DJJ (2013). Retrodeforming the Arabia-Eurasia collision zone: Age of collision versus magnitude of continental subduction. Geology 41 (3): 315–318. doi: 10.1130/g33591.1

Moghadam HS, Ghorbani G, Khedr MZ, Fazlnia N, Chiaradia M et al. (2014). Late Miocene K-rich volcanism in the Eslamieh Peninsula (Saray), NW Iran: implications for the geodynamic evolution of the Turkish–Iranian High Plateau. Gondwana Research 26: 1028–1050.

Moyen JF (2009). High Sr/Y and La/Yb ratios: the meaning of the 'adakitic signature. Lithos 112: 556–574.

MTA (2002). 1/500.000 ölçekli Türkiye Jeoloji Haritası, Erzurum, Sivas Paftaları, Maden Tetkik ve Arama Genel Müdürlüğü, Ankara (in Turkish).

Nebel O, Nebel-Jacobsen Y, Mezger K, Berndt J (2007). Initial Hf isotope compositions in magmatic zircon from early Proterozoic rocks from the Gawler Craton, Australia: A test for zircon model ages. Chemical Geology 241: 23–37.

Nichols GT, Wyllie PJ, Stern CR (1994). Subduction zone melting of pelagic sediments constrained by melting experiments. Nature 371: 785-788.

Okay AI, Zattin M, Cavazza W (2010). Apatite fission-track data for the Miocene Arabia-Eurasia collision. Geology 38 (1): 35–38.

Özkul M (1988). Elazığ batısında Kırkgeçit Formasyonu üzerinde sedimantolojik incelemeler. PhD, Fırat Üniversitesi, Elazığ, Turkey (in Turkish).

Palmer MR, Ersoy EY, Akal C, Uysal İ, Genç ŞC et al. (2019). A short, sharp pulse of potassium-rich volcanism during continental collision and subduction. Geological 47 (11): 1083–1087.

Parlak O, Çolakoğlu A, Dönmez C, Sayak H, Yıldırım N et al. (2012). Geochemistry and tectonic significance of ophiolites along the Ankara-Erzincan süture zone in northeastern Anatolia. In: Robertson AHF, Parlak O, Ünlügenç UC (editors). Geological Development of Anatolia and the Easternmost Mediterranean Region. Geological Society, London, Special Publications 372: 75-105.

Patiño Douce AE, Beard JS (1996). Effects of P, f(O2) and Mg/Fe Ratio on Dehydration Melting of Model Metagreywackes. Journal of Petrology 37: 999-1024.

Pearce JA, Bender JF, De Long SE, Kidd WSF, Low PJ et al. (1990). Genesis of collision volcanism in eastern Anatolia Turkey. Journal of Volcanology and Geothermal Research 44: 189-22.

Peccerillo A, Taylor SR (1976). Geochemistry of Eocene Calc-Alkaline Volcanic Rocks from the Kastamonu area, Northern Turkey. Contributions to Mineralogy and Petrology 58: 63-81.

Petford N, Atherton M (1996). Na-rich partial melts from newly underplated basaltic crust: the Cordillera Blanca batholith. Peru. Journal of Petrology 37: 1491–1521.

Plank T, Langmuir CH (1998). The chemical composition of subducting sediment: implications for the crust and mantle. Chemical Geology 145: 325–394.

Portner DE, Delph JR, Biryol CB, Beck SL, Zandt G et al. (2018). Subduction termination through progressive slab deformation across Eastern Mediterranean subduction zones from updated P- wave tomography beneath Anatolia. Geosphere 14 (3): 907–925.

Prouteau G, Scaillet B, Pichavant M, Maury R (2001). Evidence for mantle metasomatism by hydrous silicic melts derived from subducted oceanic crust. Nature 40: 197–200.

Prouteau G, Scaillet B (2003). Experimental constraints on the origin of the 1991 Pinatubo dacite. Journal of Petrology 44: 2203–2241.

Racano S, Schildgen TF, Cosentino D, Miller SR (2021). Temporal and spatial variations in rock uplift from river-profile inversions at the Central Anatolian Plateau southern margin. Journal of Geophysical Research: Earth Surface 126: e2020JF006027. doi: 10.1029/2020JF006027

Rapp RP, Watson EB, Miller CF (1991). Partial melting of amphibolite/eclogite and the origin of Archean trondhjemites and tonalites. Precambrian Research 51: 1-25.

Rapp RP, Watson EB (1995). Dehydration melting of metabasalt at 8–32 kbar: implications for continental growth and crust-mantle recycling. Journal of Petrology 36: 891–931.

Rapp RP, Shimizu N, Norman MD (2003). Growth of early continental crust by partial melting of eclogite. Nature 425: 605–609.

Rızaoğlu T, Parlak O, Höock V, Koller F, Hames WE et al. (2009). Andean-type active margin formation in the eastern Taurides: geochemical and geochronological evidence from the Baskil granitoid (Elazığ, SE Turkey). Tectonophysics 473: 188-207.

Reid MR, Delph JR, Cosca MA, Schleiffarth WK, Kuşcu GG (2019). Melt equilibration depths as sensors of lithospheric thickness during Eurasia-Arabia collision and the uplift of the Anatolian Plateau: Geology 47: 943–947.

Rollinson HR, Tarney J (2005). Adakites-the key to understanding LILE depletion in granulites. Lithos 79: 61-81.

Rudnick RL, Gao S (2003). The Composition of the Continental Crust. In: Holland HD, Turekian KK (editors). Treatise on Geochemistry, Elsevier-Pergamon, Oxford 3: 1-64.

Sağıroğlu A, Şaşmaz A (2004). Mineralogy and geochemistry of the argentiferous Pb–Zn and Cu veins of the Çolaklı area, Elazığ, Eastern Turkey. Journal of Asian Earth Sciences 23 (1): 37-45.

Scaillet B, Evans BW (1999). The 15 June 1991 eruption of Mount Pinatubo. I. Phase equilibria and pre-eruption P–T– fO2–fH2O conditions of the dacite magma. Journal of Petrology 40: 381–411.

Skobeltsyn G, Mellors R, Gök R, Türkelli N, Yetirmishli G et al. (2014). Upper mantle S wave velocity structure of the east Anatolian-Caucasus region. Tectonics 33: 207–221.

Sun S, McDonough WF (1989). Chemical and isotopic systematics of oceanic basalts: implications for mantle composition and processes. Geological Society, London, Special Publications 42: 313–345.

Şen C, Dunn T (1994). Dehydration melting of a basaltic composition amphibolite at 1·5 and 2·0 GPa: implications for the origin of adakites. Contributions to Mineralogy and Petrology 117: 394-409.

Şen P, Şen E (2013). Petrogenetıc characterıstics of Oyaca – Kedikayası – Boyalık adakites in SW Ankara (central Anatolia, Turkey): Evidence for slab melt metasomatism. Bulletin of the Mineral Research and Exploration 146: 81-92.

Şengör AMC, Yılmaz Y (1981). Tethyan Evolution of Turkey: A Plate Tectonic Approach. Tectonophysics 75: 181-241.

Şengör A, Özeren S, Genç T, Zor E (2003). East Anatolian high plateau as a mantle supported, north-south shortened domal structure, Geophysical Research Letters 30 (24): 8045.

Şengör AMC, Özeren MS, Keskin M, Sakınç M, Özbakır AD et al. (2008). Eastern Turkish high plateau as a small Turkic-type orogen: Implications for post-collisional crust-forming processes in Turkic-type orogens. Earth-Science Reviews 90 (1): 1–48.

Topuz G, Okay AI, Altherr R, Schwarz WH, Siebel W et al. (2011). Post-collisional adakite-like magmatism in the Ağvanis massif and implications for the evolution of the Eocene magmatism in the Eastern Pontides (NE Turkey). Lithos 125: 131–150.

Topuz G, Candan O, Zack T, Chen F, Li QL (2019). Origin and significance of Early Miocene high-potassium I-type granite plutonism in the East Anatolian plateau (the Taşlıçay intrusion). Lithos 348-349: 105210.

Tsuchiya N, Suzuki S, Kimura JI, Kagami H (2005). Evidence for slab melt/mantle reaction: Petrogenesis of early Cretaceous and Eocene high-Mg andesites from the Kitakami Mountains, Japan. Lithos 79: 179–206.

Ural M, Arslan M, Göncüoglu MC, Tekin UK, Kürüm S (2015). Late Cretaceous arc and back-arc formation within the southern Neotethys: whole-rock, trace element, and Sr-Nd-Pb isotopic data from basaltic rocks of the Yüksekova complex (Malatya-Elazığ, SE Turkey). Ofioliti 40 (1): 57-72.

Varol E, Temel A, Gourgaud A, Bellon H (2007). Early Miocene 'adakite-like' volcanism in the Balkuyumcu region, central Anatolia, Turkey: petrology and geochemistry. Journal of Asian Earth Sciences 30: 613-628.

Wang Y, Foley SF (2018). Hybridization Melting between continent-derived sediment and depleted peridotite in subduction zones. Journal of Geophysical Research: Solid Earth 123. doi: 10.1029/2018JB015507

Wang Q, McDermott F, Xu JF, Bellon H, Zhu YT (2005). Cenozoic K-rich adakitic volcanic rocks in the Hohxil area, northern Tibet: Lower-crustal melting in an intracontinental setting. Geology 33: 465–468.

Wang Q, Xu JF, Jian P, Bao ZW, Zhao ZH et al. (2006). Petrogenesis of adakitic porphyries in an extensional tectonic setting, dexing, south China: Implications for the genesis of porphyry copper mineralization. Journal of Petrology 47 (1): 119-144.

Wang Q, Wyman DA, Xu J, Jian P, Zhao Z et al. (2007). Early Cretaceous adakitic granites in the Northern Dabie Complex, central China: implications for partial melting and delamination of the thickened lower crust. Geochimica et Cosmochimica Acta 71: 2609–2636.

Wang Y, Foley SF, Prelević D (2017). Potassium-rich magmatism from a phlogopite-free source. Geology 45: 467-470.

Woodhead JD, Hergt JM, Davidson JP, Eggins SM (2001). Hafnium isotope evidence for 'conservative' element mobility during subduction processes. Earth and Planetary Science Letters 192: 331-346.

Xu JF, Shinjo S, Defant MJ, Wang Q, Rapp RP (2002). Origin of Mesozoic adakitic intrusive rocks in the Ningzhen area of east China: partial melting of delaminated lower continental crust? Geology 30: 1111-1114.

Xu YG, Lan JB, Yang QJ, Huang XL, Qiu HN (2008). Eocene break-off of the Neo-Tethyan slab as inferred from intraplate-type mafic dykes in the Gaoligong orogenic belt, eastern Tibet. Chemical Geology 255: 439-453.

Yalçın H, Gündoğdu MN, Gourgaud A, Vidal P, Uçurum A (1998). Geochemical characteristics of Yamadag˘ı volcanics in central east Anatolia: an example from collision-zone volcanism. Journal of Volcanology and Geothermal Research 85: 303–326.

Yılmaz Y, Şaroğlu F, Güner Y (1987). Initiation of the neomagmatism in east Anatolia. Tectonophysics 134: 177-199.

Yılmaz Y, Güner Y, Şaroğlu F (1998). Geology of the Quaternary volcanic centers of East Anatolia. Journal of Volcanology and Geothermal Research 85: 173-210.

Yılmaz H, Alpaslan M, Temel A (2007). Two-stage felsic volcanism in the western part of the southeastern Anatolian orogen: petrologic and geodynamic implications. International Geology Review 49: 120-141.

Yılmaz-Şahin S, Aysal N, Güngör Y (2012). Petrogenesis of late cretaceous adakitic magmatism in the İstanbul zone (Çavuşbaşı Granodiorite, NW Turkey). Turkish Journal of Earth Sciences 21: 1029-1045.

Yogodzinski GM, Less JM, Churikova TG, Dorendof F, Wörner G et al. (2001). Geochemical evidence for the melting of subducting oceanic lithosphere at plate edges. Nature 409: 500-504.

Yumul Jr GP, Dimalanta CB, Faustino DV (1999). Silicic arc volcanism and lower crust melting: an example from the central Luzon, Philippines. Journal of Geology 154: 13-14.

Yücel C (2018). Geochronology, geochemistry, and petrology of adakitic Pliocene–Quaternary volcanism in the Şebinkarahisar (Giresun) area, NE Turkey. Internatıonal Geology Review 61 (6): 754-777.

Zhang Q, Wang Y, Qian Q, Yang JH, Wang YL et al. (2001). The characteristics and tectonic-metallogenic significances of the adakites in Yanshan period from eastern China. Acta Petrologica Sinica 17: 236-244.

Zhang LY, Ducea MN, Ding L, Pullen A, Kapp P et al. (2014). Southern Tibetan Oligocene–Miocene adakites: A record of Indian slab tearing. Lithos 210–211: 209-223.

Zhou Z (1986). The origin of intrusive mass in Fengshandong, Hubei province. Acta Petrologica Sinica 2: 59–70. (In Chinese with English Abstract).

Zhu G, Liu GS, Niu ML, Xie CL, Wang YS et al. (2009). Syn-collisional transform faulting of the Tan-Lu fault zone, East China. International Journal of Earth Sciences (Geology Rundsch) 98: 135-155.

Zor E (2008). Tomographic evidence of slab detachment beneath eastern Turkey and the Caucasus. Geophysical Journal International 175: 1273–1282.

Appendix Table 1. Plagioclase composition.

Dacite / Tracydacite–Plagioclase (P2)																			
Sample no	P2-1	P2-2	P2-3	P2-4	P2-5	P2-6	P2-7	P2-8	P2-9	P2-10	P2-11	P2-12	P2-13	P2-14	P2-15	P2-16	P2-17	P2-18	P2-19
SiO2	57.24	57.25	56.33	64.37	51.36	54.95	60.70	62.87	58.36	57.92	58.52	58.35	61.25	59.03	54.52	59.24	60.80	56.12	55.16
Al2O3	22.18	22.17	21.93	24.97	20.16	21.17	22.99	23.76	22.92	21.93	22.50	23.01	23.96	22.51	21.38	22.24	23.16	22.09	21.72
FeO	0.00	0.26	0.00	0.00	0.27	0.00	0.00	0.00	0.00	0.04	0.20	0.00	0.00	0.07	0.03	0.00	0.00	0.30	0.00
CaO	4.73	4.67	4.85	4.93	6.06	4.83	5.31	4.81	5.11	4.63	5.45	5.48	5.05	5.51	4.86	4.83	5.17	5.11	4.92
Na2O	9.46	8.4	7.31	8.27	5.18	8.08	7.62	6.91	7.48	8.77	9.40	7.61	7.48	6.13	9.65	9.05	9.23	9.61	8.29
K2O	0.47	0.53	0.66	0.42	0.69	0.50	0.59	0.39	0.60	0.64	0.72	0.56	0.48	0.72	0.80	0.65	0.66	0.59	0.50
On the basis of 32 oxygen																			
Si	10.89	10.93	10.98	11.05	10.92	10.94	11.07	11.19	10.96	11.00	10.86	10.92	11.02	11.10	10.77	11.01	10.96	10.77	10.87
Al	4.97	4.99	5.04	5.05	5.05	4.97	4.94	4.98	5.07	4.91	4.92	5.08	5.08	4.99	4.98	4.87	4.92	5.00	5.04
Fe(ii)	0.00	0.04	0.00	0.00	0.05	0.00	0.00	0.00	0.00	0.01	0.03	0.00	0.00	0.01	0.01	0.00	0.00	0.05	0.00
Ca	0.96	0.96	1.01	0.91	1.38	1.03	1.04	0.92	1.03	0.94	1.08	1.10	0.97	1.11	1.03	0.96	1.00	1.05	1.04
Na	3.49	3.16	2.76	2.75	2.13	3.12	2.69	2.38	2.73	3.23	3.38	2.76	2.61	2.23	3.70	3.26	3.23	3.58	3.17
K	0.11	0.13	0.16	0.09	0.19	0.13	0.14	0.09	014	0.15	0.17	0.13	0.11	0.17	0.20	0.15	0.15	0.15	0.13
Ba	0.00	0.00	0.00	0.00	0.00	0.00	0.00	0.00	0.00	0.00	0.00	0.00	0.00	0.00	0.00	0.00	0.00	0.00	0.00
Total	20.43	20.22	19.96	19.85	19.72	20.19	19.88	19.56	19.94	20.24	20.45	19.99	19.80	19.61	20.69	20.26	20.26	20.59	20.25
An mol %	21.10	22.51	25.73	24.18	37.27	24.11	26.79	27.05	26.39	21.79	23.38	27.52	2636	31.56	20.87	21.97	22.82	22.01	23.98
Ab mol %	76.39	74.45	70.11	73.36	57.66	72.92	69.66	70.35	69.94	74.64	72.94	69.13	70.63	63.50	75.02	74.50	73.73	74.94	73.13
Or mol %	2.51	3.04	4.16	2.46	5.07	2.98	3.55	2.59	3.67	3.58	3.68	3.34	3.01	4.93	4.11	3.53	3.45	3.05	2.89
Sample no	P2-20	P2-21	P2-22	P2-23	P2-24	P2-25													
SiO2	64.66	56.83	61.14	57.29	57.11	60.94													
Al2O3	19.91	21.83	23.21	22.52	21.87	24.82													
FeO	0.00	0.00	0.47	0.00	0.07	0.26													
CaO	5.30	5.24	5.40	4.87	6.95	5.11													
Na2O	6.32	9.09	8.75	8.91	6.32	8.49													
K2O	0.50	0.70	0.53	0.50	0.44	0.40													
On the basis of 32 oxygen																			
Si	11.71	10.88	10.97	10.87	10.96	10.84													
Al	4.25	4.93	4.91	5.04	4.94	5.20													
Fe(ii)	0.00	0.00	0.07	0.00	0.01	0.04													

Appendix Table 1. (Continued).

Ca	1.03	1.08	1.04	0.99	1.43	0.97													
Na	2.22	3.37	3.04	3.28	2.35	2.93													
K	0.11	0.17	0.12	0.12	0.11	0.09													
Ba	0.00	0.00	0.00	0.00	0.00	0.00													
Total	19.33	20.43	20.16	20.31	19.80	20.07													
An mol %	30.61	23.27	24.68	22.57	36.74	24.39													
Ab mol %	65.98	73.03	72.43	74.70	60.50	73.35													
Or mol %	3.42	3.70	2.89	2.73	2.76	2.26													
Total iron as Fe^{+2} An: Anhortite, Ab: Albite, Ort: orthoclase.																			

Plagioclase, cont. (P6)

Tracyandesite-Plagioclase																
Sample no	P6-1	P6-2	P6-4	P6-5	P6-6	P6-7	P6-8	P6-10	P6-11	P6-12	P6-13	P6-14	P6-15	P6-16	P6-17	P6-18
SiO2	59.29	61.25	58.65	66.09	53.62	63.03	62.83	64.43	60.76	64.90	60.31	60.86	64.05	56.82	64.47	62.08
Al2O3	24.26	24.11	24.46	26.21	33.19	24.48	23.67	26.87	23.79	26.01	25.12	26.93	26.53	24.87	25.31	26.04
FeO	0.25	0.00	0.23	0.29	0.00	0.00	0.00	0.00	0.00	0.00	0.11	0.29	0.36	0.00	0.31	0.00
CaO	6.79	6.18	7.39	7.46	7.56	5.90	5.45	8.05	6.03	7.06	7.31	9.42	6.82	7.16	6.95	7.38
Na2O	8.85	7.96	7.74	5.29	5.69	7.98	7.24	7.09	6.62	6.57	7.68	5.04	7.58	6.59	6.96	6.13
K2O	0.74	0.61	0.59	0.55	0.51	0.61	0.74	0.48	0.64	0.54	0.70	0.49	0.52	0.67	0.56	0.45
On the basis of 32 oxygen																
Si	10.66	10.90	10.63	11.00	9.54	10.97	11.12	10.73	10.99	10.93	10.67	10.53	10.77	10.56	10.94	10.78
Al	5.14	5.05	5.22	5.14	6.96	5.02	4.94	5.27	5.07	5.16	5.24	5.49	5.26	5.45	5.06	5.33
Fe(ii)	0.04	0.00	0.03	0.04	0.00	0.00	0.00	0.00	0.00	0.00	0.02	0.04	0.05	0.00	0.04	0.00
Ca	1.31	1.18	1.44	1.33	1.44	1.10	103	1.44	1.17	1.27	1.39	1.75	1.23	1.43	1.26	1.37
Na	3.08	2.75	2.72	1.71	1.96	269	2.48	2.29	2.32	2.14	2.63	1.69	2.47	2.38	2.29	2.06
K	0.17	014	0.14	0.12	0.12	0.14	0.17	0.10	0.15	0.11	0.16	0.11	0.11	0.16	0.12	0.10
Ba	0.00	0.00	0.00	0.00	0.00	0.00	0.00	0.00	0.00	0.00	0.00	0.00	0.00	0.00	0.00	0.00
Total	20.40	20.02	20.18	19.34	20.02	19.93	1974	19.83	19.71	19.62	20.11	19.62	19.89	19.98	19.73	19.64
An	28.65	29.00	33.44	42.17	40.91	2802	28.05	37.53	32.14	36.03	33.17	49.26	32.23	35.99	34.38	38.81
Ab	67.62	67.57	63.36	54.,11	55.78	6851	67.41	59.78	63.81	60.72	63.06	47.71	64.84	59.99	62.31	58.40
Or	3.74	3.43	3.20	3.73	3.31	3.47	4.54	2.69	4.05	3.25	3.77	3.03	2.92	4.02	3.32	2.79

Appendix Table 1. (Continued).

Sample no	P6-20	P6-21	P6-22	P6-23	P6-24	P6-25										
SiO2	58.,37	67.23	61.54	64.14	58.31	60.72										
Al2O3	25.,25	27.38	23.93	26.17	2378	26.48										
FeO	0.08	0.11	0.00	0.00	0.07	0.16										
CaO	8.01	7.44	6.86	7.13	6.55	8.89										
Na2O	6.61	5.73	7.15	796	7.83	6.12										
K2O	0.48	0.46	0.75	0.49	0.52	0.61										
On the basis of 32 oxygen																
Si	10.57	10.93	10.93	10.79	10.74	10.55										
Al	5.39	5.25	5.01	5.19	5.16	5.42										
Fe(ii)	0.01	0.01	0.00	0.00	0.01	0.02										
Ca	1.55	1.30	1.31	1.29	1.29	1.65										
Na	2.32	1.81	2.46	2.60	2.80	2.06										
K	0.11	010	0.17	0.11	0.12	0.14										
Ba	0.00	0.00	0.00	0.00	0.00	0.00										
Total	19.95	19.40	19.88	19.97	20.13	19.84										
An	38.97	40.51	33.17	32.24	30.70	42.94										
Ab	58.27	56.52	62.53	65.10	66.41	53.55										
Or	2.76	2.98	4.30	2.66	2.89	3.51										

Plagioclase, cont. (P9)

Tracydacite-Plagioclase																				
Sample no	P9-1	P9-2	P9-3	P9-4	P9-5	P9-6	P9-7	P9-9	P9-10	P9-11	P9-12	P9-13	P9-14	P9-15	P9-17	P9-19	P9-20	P9-22	P9-23	P9-24
SiO2	65.05	56.10	66.69	59.22	64.84	53.84	58.94	62.33	59.69	58.01	61.99	60.35	60.99	63.64	54.86	59.02	57.79	58.29	62.88	62.60
Al2O3	25.79	21.00	24.14	24.24	24.55	21.64	22.68	23.29	25.32	23.41	24.49	23.11	24.79	26.18	24.20	24.43	24.20	24.85	25.70	23.90
FeO	0.00	4.15	0.17	0.01	0.00	0.17	0.05	0.31	0.19	0.19	0.23	0.16	0.52	0.26	0.09	0.01	0.38	0.22	0.03	0.09
CaO	6.87	5.79	6.61	6.80	5.61	11.85	7.60	5.29	7.73	6.73	6.90	6.24	6.97	6.89	8.06	6.95	7.47	7.08	8.48	6.37
Na2O	5.41	7.26	5.74	7.86	7.24	4.47	6.33	8.41	6.31	7.05	6.95	6.90	7.46	8.60	7.94	7.34	7.18	7.46	5.74	6.82
K2O	0.48	0.81	0.68	0.66	0.43	0.61	0.68	0.53	0.52	0.57	0.55	0.65	0.47	0.52	0.49	0.43	0.28	0.50	0.47	0.56
On the basis of 32 oxygen																				
Si	11.04	10.78	11.27	10.73	11.13	10.54	10.92	11.06	10.67	10.79	10.90	11.00	10.77	10.73	10.37	10.73	10.64	10.61	10.81	11.05
Al	5.16	4.75	4.81	5.17	4.97	4.99	4.95	4.87	5.33	5.13	5.08	4.97	5.16	5.20	5.39	5.23	5.25	5.33	5.21	4.97

Appendix Table 1. (Continued).

Fe(ii)	0.00	0.67	0.02	0.00	0.00	0.03	0.01	0.05	0.03	0.03	0.03	0.02	0.08	0.,04	0.01	0.00	0.06	0.03	0.00	0.01
Ca	1.25	1.19	1.20	1.32	1.03	2.49	1.51	1.01	1.48	1.34	1.30	1.22	1.32	1.24	1.63	1.35	1.47	1.38	1.56	1.20
Na	1.78	2.70	1.88	2.76	2.41	1.70	2.27	2.89	2.19	2.54	2.37	2.44	2.55	2.81	2.91	2.59	2.56	2.63	1.91	2.33
K	0.10	0.20	0.15	0.15	0.10	0.15	0.16	0.12	0.12	0.13	0.12	0.15	0.11	0.11	0.12	0.10	0.07	0.12	0.10	0.13
Ba	0.00	0.00	0.00	0.00	0.00	0.00	0.00	0.00	0.00	0.00	0.00	0.00	0.00	0.00	0.00	0.00	0.00	0.00	0.00	0.00
Total	19.33	20.30	19.33	20.14	19.64	19.89	19.82	20.01	19.82	19.98	19.81	19.81	19.98	20.13	20.44	20.00	20.05	20.10	19.60	19.70
An	39.84	29.11	37.11	31.19	29.16	57.35	38.27	25.03	39.12	33.39	34.28	32.01	33.13	29.87	35.02	33.50	35.90	33.44	43.67	32.88
Ab	56.83	66.03	58.35	65.21	68.15	39.15	57.65	71.98	57.78	63.27	62.48	64.04	64.21	67.42	62.45	64.05	62.47	63.77	53.48	63.67
Or	3.33	4.86	4.54	3.59	2.69	3.50	4.08	2.98	3.11	3.35	3.24	3.95	2.67	2.70	2.53	2.45	1.63	2.79	2.85	3.45

Plagioclase, cont. (P11)

Tracydacite-Plagioclase																			
Sample	P11-1	P11-2	P11-3	P11-4	P11-5	P11-6	P11-7	P11-8	P11-9	P11-10	P11-11	P11-12	P11-13	P11-14	P11-15	P11-16	P11-17	P11-18	P11-19
SiO2	57.05	55.46	56.84	57.90	56.94	50.71	57.96	52.22	53.68	53.24	59.37	55.14	56.63	55.81	58.50	55.57	58.22	51.54	58.76
Al2O3	25.68	24.86	26.17	26.56	26.61	22.85	26.06	24.70	23.96	24.52	26.39	25.58	25.99	26.08	26.81	26.18	25.60	24.03	25.98
FeO	0.24	0.00	0.44	0.33	0.00	0.14	0.29	0.40	0.00	0.00	0.24	0.00	0.48	0.12	0.35	0.01	0.10	0.44	0.27
CaO	9.08	8.94	8.75	9.58	9.63	7.19	8.65	12.05	8.07	9.03	8.62	9.50	8.58	9.52	9.34	9.79	8.52	7.65	9.27
Na2O	5.70	5.35	6.29	4.85	5.59	6.58	5.44	5.18	5.66	6.93	5.05	5.37	5.77	5.73	5.76	5.64	4.36	6.35	5.39
K2O	0.37	0.57	0.43	0.43	0.37	0.33	0.33	0.40	0.31	0.59	0.40	0.32	0.39	0.44	0.35	0.45	0.38	0.48	0.49
On the basis of 32 oxygen																			
Si	10.42	10.44	10.33	10.39	10.30	10.39	10.48	10.03	10.47	10.22	10.56	10.31	10.38	10.27	10.37	10.24	10.62	10.27	10.50
Al	5.53	5.51	5.60	5.62	5.67	5.52	5.55	5.59	5.51	5.55	5.53	5.64	5.61	5.66	5.60	5.68	5.50	5.64	5.47
Fe(ii)	0.04	0.00	0.07	0.05	0.00	0.02	0.04	0.06	0.00	0.00	0.04	0.00	0.07	0.02	0.05	0.00	0.01	0.07	0.04
Ca	1.78	1.80	1.70	1.84	1.87	1.58	1.68	2.48	1.69	1.86	1.64	1.90	1.68	1.88	1.77	1.93	1.66	1.63	1.77
Na	2.02	1.95	2.22	1.69	1.96	2.61	1.91	1.93	2.14	2.58	1.74	1.95	2.05	2.04	1.98	2.02	1.54	2.45	1.87
K	0.09	0.4	0.10	0.10	0.08	0.09	0.08	0.10	0.08	0.14	0.09	0.08	0.09	0.10	0.08	0.11	0.09	0.12	0.11
Ba	0.00	0.,00	0.00	0.00	0.00	0.00	0.00	0.00	0.00	0.00	0.00	0.00	0.00	0.00	0.00	0.00	0.00	0.00	0.00
Total	19..87	19.85	20.02	19.69	19.89	20.21	19.74	20.19	19.89	20.36	19.60	19.88	19.89	19.97	19.86	19.98	19.44	20.20	19.76
An	4579	46.34	42.38	50.79	47.69	36.90	45.83	55.01	43.20	40.53	47.29	48.48	44.04	46.63	46.29	47.65	50.53	38.83	47.28
Ab	51.99	50.16	55.15	46.51	50.14	61.06	52.10	42.83	54.83	56.30	50.08	49.59	53.55	50.81	51.65	49.71	46.80	58.30	49.73
Or	2.22	3.50	2.47	2.70	2.17	2.04	2.07	2.16	1.97	3.16	2.63	1.93	2.41	2.56	2.06	2.63	2.67	2.87	2.99

Appendix Table 1. (Continued).

Sample	P11-20	P11-21	P11-22	P11-23	P11-24	P11-25													
SiO2	55.03	55.47	51.42	55.85	53.01	55.48													
Al2O3	25.53	24.96	28.59	27.47	24.03	25.04													
FeO	0.00	0.26	0.00	0.43	0.21	0.24													
CaO	9.22	9.50	8.72	9.36	8.45	8.72													
Na2O	5.88	5.83	4.83	5.24	6.58	5.92													
K2O	0.41	0.53	0.36	0.49	0.42	0.52													
On the basis of 32 oxygen																			
Si	10.30	10.35	9.81	10.15	10.32	10.39													
Al	5.63	5.49	6.43	5.88	5.51	5.53													
Fe(ii)	0.00	0.04	0.00	0.07	0.03	0.04													
Ca	1.85	1.90	1.78	1.82	1.76	1.75													
Na	2.13	2.11	1.79	1.85	2.48	2.15													
K	0.10	0.13	0.09	0.11	0.11	0.12													
Ba	0.00	0.00	0.00	0.00	0.00	0.00													
Total	20.01	20.02	19.91	19.89	20.22	19.98													
An	45.29	45.95	48.73	48.18	40.52	43.49													
Ab	52.30	51.02	48.88	48.82	57.06	53.45													
Or	2.41	3.04	2.39	3.00	2.42	3.07													

Plagioclase, cont. (P19)

Dacite / Tracydacite-Plagioclase																		
Sample	P19-1	P19-2	P19-3	P19-4	P19-5	P19-6	P19-7	P19-8	P19-9	P19-10	P19-11	P19-12	P19-13	P19-14	P19-16	P19-17	P19-18	P19-19
SiO2	66.27	55.57	52.34	54.36	56.98	57.10	59.34	54.61	60.69	57.29	57.80	59.53	53.13	55.40	62.98	50.29	57.24	55.93
Al2O3	28.74	23.14	22.45	21.00	22.23	24.29	24.62	23.09	23.98	22.44	25.46	25.41	23.80	24.27	26.13	21.51	23.69	22.97
FeO	0.09	0.16	0.37	0.29	0.39	0.14	0.00	0.00	0.00	0.00	0.00	0.04	0.00	0.10	0.00	0.00	0.27	0.60
CaO	7.49	6.43	5.99	4.73	4.85	6.34	6.35	6.65	5.31	5.74	6.86	7.12	6.73	7.57	6.89	6.09	7.08	6.40
Na2O	7.66	6.42	8.22	7.67	8.12	6.45	6.89	7.38	8.54	7.66	6.53	4.27	7.69	6.65	5.60	6.87	6.07	6.77
K2O	0.83	0.43	0.53	0.57	0.51	0.26	0.49	0.54	0.33	0.50	0.30	0.33	0.55	0.40	0.34	0.25	0.54	0.51
On the basis of 32 oxygen																		
Si	10.64	10.74	10.51	10.94	10.92	10.72	10.79	10.61	10.91	10.90	10.60	10.82	10.41	10.51	10.88	10.59	10.75	10.74
Al	5.43	5.27	5.31	4.98	5.02	5.37	5.28	5.29	5.08	5.03	5.50	5.45	5.49	5.43	5.32	5.34	5.24	5.20

Appendix Table 1. (Continued).

Fe(ii)	0.01	0.03	0.06	0.05	0.06	0.02	0.00	0.00	0.00	0.00	0.00	0.01	0.00	0.02	0.00	0.00	0.04	0.10
Ca	1.29	1.33	1.29	1.02	1.00	1.27	1.24	1.38	1.02	1.17	1.35	1.39	1.41	1.54	1.28	1.37	1.42	1.,32
Na	2.38	2.40	3.20	2.99	3.02	2.35	2.43	2.78	2.98	2.82	2.32	1.51	2.92	2.45	1.88	2.81	2.21	2.52
K	0.17	0.11	0.14	0.15	0.13	0.06	0.11	0.13	0.08	0.12	0.07	0.08	0.14	0.10	0.07	0.07	0.13	0.12
Ba	0.00	0.00	0.00	0.00	0.00	0.00	0.00	0.00	0.00	0.00	0.00	0.00	0.00	0.00	0.00	0.00	0.00	0.00
Total	19.92	19.88	20.50	20.13	20.14	19.80	19.84	20.20	20.07	20.05	19.85	19.25	20.37	20.04	19.43	20.18	19.80	19.99
An	33.50	34.64	27.89	24.53	24.05	34.59	32.3	32.21	25.10	28.43	36.05	46.71	31.60	37.69	39.56	32.34	37.83	33.21
Ab	62.06	62.61	69.19	71.95	72.92	63.71	64.27	64.70	73.03	68.62	62.09	50.75	65.31	59.94	58.15	66.05	58.75	63.66
Or	4.44	2.75	2.92	3.52	3.03	1.69	3.00	3.10	1.88	2.95	1.86	2.54	3.10	2.37	2.29	1.61	3.42	3.12
Sample no	P19-20	P19-21	P19-22	P19-23	P19-24	P19-25												
SiO2	57.27	59.10	54.31	56.07	55.03	57.79												
Al2O3	22.23	22.74	23.27	22.93	21.92	23.62												
FeO	0.00	0.02	0.00	0.35	0.08	0.15												
CaO	5.50	5.03	7.34	6.,64	5.25	7.07												
Na2O	7.78	7.44	8.02	5.57	8.94	7.24												
K2O	0.54	0.17	0.59	0.,43	0.43	0.56												
On the basis of 32 oxygen																		
Si	10.93	11.05	10.48	10.82	10.77	10.73												
Al	5.00	5.01	5.29	5.22	5.06	5.17												
Fe(ii)	0.00	0.00	0.00	0.06	0.,01	0.02												
Ca	1.12	1.01	1.52	1.37	1.10	1.41												
Na	2.88	2.70	3.00	2.09	3.39	2.60												
K	0.13	004	0.14	0.11	0.11	0.13												
Ba	0.00	0.00	0.00	0.00	0.00	0.00												
Total	20.07	19.81	20.44	19.66	20.45	20.06												
An	27.19	26.90	32.55	38.54	23.91	33.93												
Ab	69.62	72.02	64.35	58.50	73.76	62.86												
Or	3.19	1.07	3.10	2.96	2.33	3.21												

Appendix Table 2. Biotite composition.

Tracydacite–Biotite (P9)																			
Sample no	P9-1	P9-2	P9-3	P9-4	P9-5	P9-6	P9-7	P9-8	P9-9	P9-10	P9-11	P9-12	P9-13	P9-14	P9-15	P9-16	P9-17	P9-18	P9-19
SiO2	34.25	38.70	35.67	35.07	42.14	32.50	34.22	37.18	38.05	34.59	34.25	37.27	35.33	40.05	32.54	30.96	29.69	34.99	34.54
MgO	10.56	7.57	11.28	12.87	14.28	11.27	11.08	11.26	11.61	11.86	11.51	11.86	12.67	10.04	11.28	8.53	7.31	10.68	4.37
FeO	18.16	22.61	20.58	16.66	18.19	15.45	20.79	17.63	18.91	17.54	17.66	18.80	20.69	21.33	16.78	17.41	19.48	17.94	27.15
TiO2	3.76	4.39	4.19	4.55	4.99	3.73	4.23	4.15	4.11	4.75	4.34	4.86	2.99	4.65	4.04	5.06	3.48	4.33	5.65
Al2O3	14.31	14.05	14.73	15.61	18.47	14.52	14.49	15.47	16.10	15.08	15.01	15.44	15.88	15.67	14.70	12.35	11.12	14.38	9.52
MnO	0.00	0.45	0.49	0.00	0.00	0.06	0.33	0.00	0.00	0.00	0.00	0.00	0.74	0.06	0.00	0.03	0.45	0.00	0.21
K2O	8.28	8.98	8.20	8.60	9.11	6.90	9.01	8.63	7.83	8.66	8.78	9.15	7.82	9.59	8.22	9.31	7.19	8.61	12.93
Si	2.87	3.08	2.82	2.78	2.91	2.86	2.73	2.94	2.95	2.79	2.79	2.86	2.74	2.99	2.76	2.80	2.89	2.88	2.88
Ti	0.24	0.26	0.25	0.27	0.26	0.25	0.25	0.25	0.24	0.29	0.27	0.28	0.17	0.26	0.26	0.34	0.25	0.27	0.35
Al	0.89	0.66	0.93	0.95	0.83	0.90	1.01	0.81	0.81	0.93	0.95	0.86	1.08	0.75	0.98	0.86	0.85	0.85	0.76
Al	0.52	0.66	0.45	0.51	0.67	0.61	0.35	0.63	0.66	0.50	0.49	0.54	0.37	0.63	0.49	0.6	0.42	0.55	0.17
Fe2+	1.27	1.50	1.36	1.10	1.05	1.14	1.39	1.17	1.23	1.18	1.20	1.21	1.34	1.33	1.19	1.32	1.59	1.24	1.89
Mg	1.32	0.90	1.33	1.52	1.47	1.48	1.32	1.33	1.34	1.42	1.40	1.36	1.47	1.12	1.43	1.15	1.06	1.31	0.54
Mn	0.00	0.03	0.03	0.00	0.00	0.00	0.02	0.00	0.00	0.00	0.00	0.00	0.05	0.00	0.00	0.00	0.04	0.00	0.01
K	0.89	0.91	0.83	0.87	0.80	0.77	0.92	0.87	0.77	0.89	0.91	0.90	0.77	0.91	0.89	1.07	0.89	0.91	1.38
Total	8.00	8.00	8.00	8.00	8.00	8.00	8.00	8.00	8.00	8.00	8.00	8.00	8.00	8.00	8.00	8.00	8.00	8.00	8.00
Xannite	0.41	0.49	0.43	0.35	0.33	0.5	0.45	0.37	0.38	0.38	0.39	0.39	0.42	0.43	0.38	0.45	0.51	0.40	0.72
Xphologopite	0.42	0.29	0.42	0.49	0.46	0.46	0.43	0.42	0.42	0.46	0.45	0.44	0.45	0.36	0.46	0.39	0.34	0.42	0.21
Fe/(Fe+Mg)	0.49	0.63	0.51	0.42	0.42	0.43	0.51	0.47	0.48	0.45	0.46	0.47	0.48	0.54	0.45	0.53	0.60	0.49	0.78
Sample no	P9-20	P9-21	P9-22	P9-23	P9-24	P9-25													
SiO2	35.64	32.07	37.06	35.13	38.82	34.26													
MgO	11.90	11.48	12.05	12.36	10.37	9.67													
FeO	19.34	14.24	16.19	18.88	17.76	19.90													
TiO2	3.57	3.64	3.76	4.35	5.30	4.87													
Al2O3	15.59	14.41	14.78	15.93	15.12	14.15													
MnO	0.17	0.00	0.12	0.13	0.00	0.02													
K2O	7.96	6.86	8.04	8.16	10.63	9.20													
Si	2.83	2.86	2.99	2.76	2.97	2.81													
Ti	0.21	0.,24	0.23	0.26	0.31	0.30													
Al	0.96	0.89	0.78	0.99	0.72	0.89													

Appendix Table 2. (Continued).

Al	0.49	0.63	0.62	0.49	0.64	0.48													
Fe^{2+}	1.28	1.06	1.09	1.24	1.14	1.37													
Mg	1.41	1.53	1.45	1.45	1.18	1.18													
Mn	0.01	0.00	0.01	0.01	0.00	0.00													
K	0.81	0.78	0.83	0.82	1.04	0.96													
Total	8.00	8.00	8.00	8.00	8.00	8.00													
Xannite	0.0	0.33	0.34	0.39	0.38	0.45													
Xphologopite	0.,44	0.47	0.46	0.45	0.40	0.39													
Fe/(Fe+Mg)	0.48	0.41	0.43	0.46	0.49	0.54													

Biotitte cont. (P11)

Tracydacite - Biotite																			
Sample no	P11-1	P11-2	P11-3	P11-4	P11-5	P11-6	P11-7	P11-8	P11-9	P11-10	P11-11	P11-12	P11-13	P11-14	P11-15	P11-16	P11-17	P11-18	P11-19
SiO2	36.39	36.05	33.41	36.16	31.82	39.74	37.25	39.34	34.31	38.09	37.02	37.51	33.07	35.32	39.85	42.33	34.61	37.38	28.65
MgO	10.47	8.57	10.88	10.23	8.81	12.07	11.59	11.87	9.82	10.94	10.66	9.33	10.84	11.42	12.64	12.56	10.37	9.83	5.72
FeO	18.80	22.41	17.77	20.11	21.44	16.12	21.37	19.78	22.60	18.56	18.30	19.74	17.54	17.78	18.52	18.52	20.26	19.75	22.68
TiO2	4.02	5.01	4.30	4.23	4.26	5.43	3.62	3.14	4.04	3.75	4.92	3.72	3.04	4.02	3.77	3.76	3.69	3.55	3.27
Al2O3	16.16	15.16	15.08	15.88	13.02	17.27	16.65	17.56	14.58	15.59	17.13	15.09	14.86	15.52	16.78	16.19	15.78	15.91	10.71
MnO	0.00	0.00	0.10	0.12	0.04	0.00	0.21	0.02	0.53	0.00	0.00	0.37	0.38	0.15	0.00	0.22	0.03	0.20	0.34
K2O	8.35	9.95	9.05	8.71	9.26	9.27	8.16	7.42	9.11	7.94	8.36	8.07	6.31	8.90	7.64	8.70	7.33	7.80	8.08
Si	2.90	2.83	2.75	2.85	2.73	2.96	2.83	2.97	2.74	3.01	2.88	3.03	2.87	2.83	2.99	3.09	2.83	2.99	2.80
Ti	0.24	0.30	0.27	0.25	0.27	0.30	0.21	0.18	0.24	0.22	0.29	0.23	0.20	0.24	0.21	0.21	0.23	0.21	0.24
Al	0.86	0.87	0.98	0.89	1.00	0.74	0.96	0.86	1.02	0.77	0.83	0.75	0.93	0.93	0.79	0.71	0.94	0.80	0.96
Al	0.66	0.53	0.48	0.58	0.32	0.78	0.53	0.70	0.36	0.68	0.74	0.69	0.59	0.53	0.69	0.68	0.58	0.70	0.28
Fe2+	1,25	1.47	1.22	1.33	1.54	1.00	1.36	1.25	1.51	1.23	1.19	1.33	1.27	1.19	1.16	1.13	1.39	1..32	1.85
Mg	1.24	1.00	1.34	1.20	1.13	1.34	1.31	1.33	1.17	1.29	1.24	1.12	1.40	1.36	1.41	1.37	1.26	117	0.83
Mn	0.00	0.00	0.01	0.01	0.00	0.00	0.01	0.00	0.04	0.00	0.00	0.03	0.03	0.01	0.00	0.01	0.00	0.01	0.03
K	0.85	1.00	0.95	0.88	1.01	0.88	0.79	0.71	0.93	0.80	0.83	0.83	0.70	0.91	0.73	0.81	0.77	0.80	1.1
Total	8.00	8.00	8.00	8.00	8.00	8.00	8.00	8.00	8.00	8.00	8.00	8.00	8.00	8.00	8.00	8.00	8.00	8.00	8.00
Xann	0.40	0.49	0.40	0.43	0.51	0.32	0.42	0.38	0.49	0.38	0.38	0.42	0.39	0.38	0.36	0.35	0.43	0.41	0.62
Xphl	0.39	0.33	0.44	0.39	0.8	0.43	0.41	0.41	0.38	0.40	0.39	0.35	0.43	0.44	0.43	0.43	0.39	0.37	0.28

Appendix Table 2. (Continued).

Fe/(Fe+Mg)	0.50	0.59	0.48	0.52	0.,58	0.43	0.51	0.48	0.56	0.49	0.49	0.54	0.48	0.47	0.45	0.45	0.52	0.53	0.69
Sample no	P11-20	P11-21	P11-22	P11-23	P11-24														
SiO2	36.99	38.67	33.11	37.53	36.63														
MgO	10.86	10.37	9.82	9.05	8.99														
FeO	21.11	20.27	18.28	20.53	24.29														
TiO2	3.37	4.76	3.00	4.31	3.71														
Al2O3	16.75	16.60	15.44	15.61	15.53														
MnO	0.22	0.19	0.00	0.00	0.27														
K2O	8.16	8.51	7.48	8.22	8.79														
Si	2.85	2.94	2.85	2.99	2.85														
Ti	0.20	0.27	0.19	0.26	0.22														
Al	0.95	0.79	0.96	0.75	0.93														
Al	0.57	0.70	0.61	0.72	0.49														
Fe2+	1.36	1.29	1.31	1.37	1..58														
Mg	1.25	1.17	1.26	1.08	1.04														
Mn	0.01	0.01	0.00	0.00	0.02														
K	0.80	0.83	0.82	0.84	0.87														
Total	8.00	8.00	8.00	8.00	8.00														
Xannite	0.43	0.41	0.41	0.43	0.50														
Xphologopite	0.39	0.37	0.40	0.34	0.33														
Fe/(Fe+Mg)	0.52	0.52	0.51	0.56	0.60														

Biotitte cont. (P19)

Tracydacite-Biotite																			
Sample no	P19-1	P19-2	P19-3	P19-4	P19-5	P19-6	P19-7	P19-8	P19-9	P19-10	P19-11	P19-12	P19-13	P19-14	P19-15	P19-16	P19-17	P19-18	P19-19
SiO2	35.90	33.25	35.14	35.37	34.24	34.10	37.90	34.93	36.21	34.96	31.99	33.20	35.61	33.85	34.54	35.10	35.86	34.57	33.99
MgO	10.12	8.74	9.62	9.85	9.11	9.67	9.67	11.12	9.98	11.11	4.65	10.25	9.05	11.14	9.46	9.66	11.38	10.39	10.60
FeO	16.55	18.28	19.12	18.23	15.48	18.04	17.81	17.53	17.95	16.00	16.05	16.61	16.72	14.79	16.82	15.80	15.43	15.12	14.34
TiO2	3.72	3.05	4.42	3.97	3.17	3.33	3.64	3.22	3.35	3.98	6.23	3.63	3.82	3.39	3.26	2.69	4.98	3.49	3.84
Al2O3	16.83	13.53	14.96	15.23	14.59	15.68	16.70	15.23	15.45	15.21	12.56	14.63	13.96	14.72	14.66	14.46	14.63	15.91	14.44

Appendix Table 2. (Continued).

MnO	0.07	0.39	0.13	0.24	0.29	0.18	0.00	0.05	0.00	0.08	0.00	0.19	0.00	0.00	0.14	0.00	0.00	0.02	0.02
K2O	7.62	7.35	7.86	8.49	7.43	7.48	8.03	7.76	7.98	7.29	9.45	8.12	7.85	7.87	7.78	7.75	8.80	7.43	7.81
Si	2.95	2.97	2.91	2.91	3.04	2.89	3.04	2.90	2.99	2.94	3.05	2.86	3.08	2.92	2.99	3.06	2.93	2.96	2.97
Ti	0.23	0.20	0.28	0.25	0.21	0.21	0.22	0.20	0.21	0.25	0.45	0.24	0.25	0.22	0.21	0.18	0.31	0.22	0.25
Al	0.82	0.82	0.81	0.85	0.75	0.89	0.75	0.90	0.81	0.81	0.50	0.90	0.67	0.86	0.80	0.76	0.76	0.82	0.78
Al	0.82	0.60	0.65	0.63	0.78	0.67	0.83	0.59	0.70	0.70	0.91	0.58	0.76	0.64	0.69	0.73	0.64	0.78	0.70
Fe2+	1.14	1.37	1.32	1.25	1.15	1.28	1.19	1.22	1.24	1.12	1.28	1.20	1.21	1.07	1.22	1.15	1.05	1.08	1.05
Mg	1.24	1.16	1.19	1.21	1.21	1.22	1.15	1.37	1.23	1.39	0.66	1.32	1.17	1.43	1.22	1.26	1.39	1.32	1.38
Mn	0.01	0.03	0.01	0.02	0.02	0.01	0.00	0.00	0.00	0..01	0.00	0.01	0.00	0.00	0.01	0.00	0.00	0.00	0.00
K	0.80	0.84	0.83	0.89	0.84	0.81	0.82	0.82	0.84	0.78	1.15	0.89	0.87	0.87	0.86	0.86	0.92	0.81	0.87
Total	8.00	8.00	8.00	8.00	8.00	8.00	8.00	8.00	8.00	8.00	8.00	8.00	8.00	8.00	8.00	8.00	8.00	8.00	8.00
Xann	0.36	0.43	0.42	0.40	0.36	0.40	0.38	0.38	0.39	0.35	0.45	0.38	0.39	0.34	0.39	0.37	0.34	0.34	0.33
Xphl	0.39	0.37	0.38	0.39	0.38	0.38	0.36	0.43	0.39	0.43	0.23	0.42	0.7	0.46	0.39	0.40	0.45	0.42	0.44
Fe/(Fe+Mg)	0.48	0.54	0.53	0.51	0.49	0.51	0.51	0.47	0.50	0.45	0.66	0.48	0.,51	0.43	0.50	0.48	0.43	0.45	0.43
Sample no	P19-20	P19-21	P19-22	P19-23	P19-24	P19-25													
SiO2	34.69	29.68	35.87	35.26	36.63	35.08													
MgO	10.91	8.00	10.01	10.08	10.28	11.76													
FeO	15.17	14.68	16.53	17.20	14.16	15.23													
TiO2	3.42	3.54	3.87	3.27	3.81	3.19													
Al2O3	14.53	12.26	15.32	15.39	15.69	14.35													
MnO	0.17	0.00	0.10	0.30	0.00	0.63													
K2O	7.87	8.08	7.83	7.42	7.03	8.13													
Si	2.97	2.92	3.00	2.97	3.11	2.94													
Ti	0.22	0.26	0.24	0.21	0.24	0.20													
Al	0.81	0.82	0.76	0.82	0.64	0.86													
Al	0.65	0.60	0.75	0.70	0.93	0.55													
Fe2+	1.09	1.21	1.16	1.21	1.01	1.07													
Mg	1.39	1.17	1.25	1.27	1.30	1.47													
Mn	0.01	0.00	0.01	0.02	0.00	0.04													
K	0.86	1.01	0.84	0.80	0.76	0.87													

Appendix Table 2. (Continued).

Total	8.00	8.00	8.00	8.00	8.00	8.00													
Xannite	0.35	0.40	0.37	0.38	0.31	0.34													
Xphologopite	0.44	0.39	0.39	0.40	0.40	0.47													
Fe/(Fe+Mg)	0.44	0.51	0.48	0.49	0.44	0.42													

Biotitte cont. (P20)

Dacite / Tracydacite-Biotite																			
Sample no	P20-1	P20-2	P20-3	P20-4	P20-5	P20-6	P20-7	P20-8	P20-9	P20-10	P20-11	P20-12	P20-13	P20-14	P20-15	P20-16	P20-17	P20-18	P20-19
SiO2	39.19	33.80	36.37	36.40	36.15	33.64	33.37	34.11	34.51	35.61	33.50	35.80	33.08	35.97	31.83	35.98	33.78	33.54	36.26
MgO	8.16	11.77	10.25	10.67	7.42	11.26	10.72	11.27	12.13	11.09	9.91	11.91	11.27	8.24	10.55	10.15	10.40	10.82	10.53
FeO	17.69	15.50	14.64	13.29	14.56	14.22	13.59	13.80	14.96	13.50	13.74	16.02	13.70	16.53	13.97	13.45	15.70	14.47	15.66
TiO2	4.07	3.46	3.07	3.78	3.37	3.45	3.03	2.73	2.74	3.12	3.77	2.61	2.85	3.54	3.56	2.95	3.15	3.22	2.53
Al2O3	14.09	14.83	14.10	12.76	12.27	14.39	13.84	13.85	15.41	15.18	13.59	14.36	14.07	14.05	14.08	14.81	13.60	14.16	13.89
MnO	0.01	0.43	0.00	0.10	0.,24	0.08	0.00	0.00	0.01	0.00	0.11	0.52	0.00	0.00	0.24	0.00	0.00	0.10	0.54
K2O	8.78	6.60	6.95	7.80	6.55	6.85	7.20	5.71	4.94	5.23	7.38	5.89	5.13	5.67	5.38	6.35	7.25	6.95	6.52
Si	3.23	2.90	3.17	3.19	3.40	2.97	3.02	3.10	3.01	3.15	3.04	3.05	3.06	3.25	2.98	3.19	3.00	2.99	3.15
Ti	0.25	0.22	0.20	0.25	0.24	0.23	0.21	0.19	0.18	0.21	0.26	0.17	0.20	0.24	0.25	0.20	0.21	0.22	0.17
Al	0.52	0.87	0.63	0.56	0.36	0.80	0.78	0.72	0.81	0.64	0.70	0.78	0.75	0.51	0.77	0.61	0.79	0.80	0.69
Al	0.85	0.63	0.82	0.75	1.01	0.69	0.70	0.76	0.78	0.95	0.75	0.66	0.78	0.99	0.78	0.94	0.63	0.69	0.74
Fe2+	1.22	1.11	1.07	0.97	1.15	1.05	1.03	1.05	1.09	1.00	1.04	1.14	1.06	1.25	1.09	1.00	1.17	1.08	1.14
Mg	1.00	1.51	1.33	1.39	1.04	1.48	1.45	1.53	1.58	1.46	1.34	1.51	1.55	1.11	1.47	1.34	1.38	1.44	1.36
Mn	0.00	0.03	0.00	0.01	0.02	0.01	0.00	0.00	0.00	0.00	0.01	0.04	0.00	0.00	0.02	0.00	0.00	0.01	0.04
K	0.92	0.72	0.77	0.87	0.79	0.77	0.83	0.66	0.55	0.59	0.85	0.64	0.60	0.65	0.64	0.72	0.82	0.79	0.72
Total	8.00	8.00	8.00	8.00	8.00	8.00	8.00	8.00	8.00	8.00	8.00	8.00	8.00	8.00	8.00	8.00	8.00	8.00	8.00
Xannite	0.40	0.34	0.33	0.31	0.36	0.32	0.32	0.31	0.32	0.29	0.33	0.34	0.31	0.37	0.33	0.30	0.37	0.34	0.35
Xphologopite	0.33	0.46	0.41	0.45	0.32	0.46	0.46	0.46	0.46	0.43	0.43	0.45	0.46	0.33	0.44	0.41	0.43	0.45	0.42
Fe/(Fe+Mg)	0.55	0.42	0.44	0.41	0.52	0.41	0.42	0.41	0.41	0.41	0.44	0.43	0.41	0.53	0.43	0.43	0.46	0.43	0.45
Sample no	P20-20	P20-21	P20-22	P20-23	P20-24	P20-25													
SiO2	35.42	33.70	32.27	36.15	35.35	36.15													
MgO	7.02	11.77	9.16	9.10	10.36	10.73													
FeO	16.52	14.67	15.24	15.90	14.01	15.96													

Appendix Table 2. (Continued).

TiO2	3.76	2.66	3.08	3.80	3.54	3.43													
Al2O3	12.76	14.83	13.07	13.23	14.00	14.63													
MnO	0.00	0.13	0.13	0.43	0.00	0.00													
K2O	6.65	6.72	7.72	7.01	5.54	5.50													
Si	3.29	2.94	2.99	3.19	3.19	3.13													
Ti	0.26	0.17	0.21	0.25	0.24	0.22													
Al	0.44	0.88	0.80	0.56	0.57	0.64													
Al	0.95	0.64	0.63	0.81	0.91	0.85													
Fe2+	1.28	1.07	1.18	1.17	1.06	1.16													
Mg	0.97	1.53	1.26	1.20	1.39	1.39													
Mn	0.00	0.01	0.01	0.03	0.00	0.00													
K	0.79	0.75	0.91	0.79	0.64	0.61													
Total	8.00	8.00	8.00	8.00	8.00	8.00													
Xannite	0.40	0.33	0.38	0.36	0.31	0.34													
Xphologopite	0.30	0.47	0.41	0.37	0.41	0.41													
Fe/(Fe+Mg)	0.57	0.41	0.48	0.49	0.43	0.45													

Appendix Table 3. Amphibole composition.

Tracydacite-Amphibole (P9)																							
Sample	P9-1	P9-2	P9-3	P9-4	P9-5	P9-6	P9-7	P9-8	P9-9	P9-10	P9-11	P9-12	P9-13	P9-14	P9-15	P9-16	P9-17	P9-18	P9-19	P9-20	P9-21	P9-22	P9-23
SiO2	41.6	33.7	39.7	42.1	45.4	38.2	43.4	38.6	37.6	40.4	42.1	45.2	42.4	36.7	39.3	38.7	39.7	40.5	29.5	45.4	44.7	38.7	44.0
TiO2	1.35	1.50	1.68	1.08	1.69	1.98	1.91	1.50	1.89	1.62	1.43	1.84	1.54	1.73	1.12	0.99	1.83	1.83	3.02	1.66	0.75	1.22	1.14
Al2O3	14.0	22.7	13.9	14.3	13.4	93.3	14.6	14.1	13.9	14.4	14.5	14.6	14.9	11.6	13.4	14.1	13.5	12.5	6.90	12.6	13.2	13.7	14.7
FeO	22.4	17.2	19.8	20.1	21.9	24.6	23.0	21.3	18.4	19.7	21.3	23.6	19.9	21.8	19.9	20.9	20.7	17.8	27.1	14.7	12.1	20.3	22.6
MnO	0.46	0.37	0.01	0.10	0.10	0.64	0.15	0.19	0.00	0.43	0.31	0.15	0.06	0.31	0.32	0.29	0.10	0.08	0.17	0.07	0.39	0.29	0.51
MgO	6.89	7.07	8.06	7.97	5.49	40.6	7.34	8.23	8.51	8.76	8.28	6.23	8.18	5.63	7.80	8.13	6.88	7.71	2.23	8.80	5.59	6.78	7.44
CaO	11.1	9.68	11.1	11.0	12.3	15.4	11.4	10.7	10.7	10.4	10.2	13.0	11.8	11.7	11.0	10.5	11.6	9.47	17.4	11.7	7.63	10.7	11.1
Na2O	1.09	2.06	2.07	1.65	0.00	11.5	1.10	2.57	2.74	2.55	1.98	0.42	1.88	0.07	1.98	2.07	1.40	2.12	0.01	1.31	4.24	1.19	1.35
K2O	1.34	1.27	1.44	1.48	1.38	2.34	1.42	1.55	1.46	1.35	1.29	1.68	1.74	1.47	1.40	1.39	1.49	1.03	2.39	1.41	1.25	1.42	1.49
On the basis of 32 oxygen																							
Si	6.11	5.05	6.01	6.19	6.62	2.15	6.11	5.80	5.85	5.94	6.03	6.32	6.13	6.07	6.05	5.85	6.10	6.34	5.56	6.71	7.06	6.06	6.17
Al^{IV}	1.89	2.95	1.99	1.81	1.38	5.85	1.89	2.20	2.15	2.06	1.97	1.68	1.87	1.93	1.95	2.15	1.90	1.66	1.53	1.29	0.94	1.94	1.83
Al^{VI}	0.53	1.05	0.48	0.66	0.93	0.33	0.53	0.29	0.40	0.43	0.48	0.74	0.66	0.34	0.47	0.37	0.54	0.64	0.00	0.90	1.51	0.58	0.61
Fe^{+3}	0.99	1.62	0.65	0.70	0.00	1.15	0.95	1.07	0.60	1.02	1.24	0.23	0.36	0.69	0.73	1.28	0.42	0.56	0.00	0.00	0.00	0.86	0.99
Ti	0.15	0.17	0.19	0.12	0.19	0.08	0.20	0.17	0.22	0.18	0.15	0.19	0.17	0.22	0.13	0.11	0.21	0.22	0.43	0.18	0.09	0.14	0.12
Cr	0.00	0.00	0.00	0.00	0.00	0.00	0.00	0.00	0.00	0.00	0.00	0.00	0.00	0.00	0.00	0.00	0.00	0.00	0.00	0.00	0.00	0.00	0.00
Fe^{+2}	1.76	0.54	1.86	1.77	2.67	0.00	1.75	1.60	1.80	1.41	1.31	2.52	2.04	2.33	1.83	1.36	2.23	1.77	4.27	1.82	1.59	1.80	1.66
Mn	0.06	0.05	0.00	0.01	0.01	0.03	0.02	0.02	0.00	0.05	0.04	0.02	0.01	0.04	0.04	0.04	0.01	0.01	0.03	0.01	0.05	0.04	0.06
Mg	1.51	1.58	1.82	1.75	1.19	3.40	1.54	1.84	1.98	1.92	1.77	1.30	1.76	1.39	1.79	1.83	1.58	1.80	0.63	1.94	1.31	1.58	1.56
Ca	1.75	1.55	1.79	1.74	1.93	0.93	1.72	1.73	1.79	1.64	1.57	1.95	1.83	2.07	1.81	1.70	1.90	1.59	3.52	1.85	1.29	1.79	1.67
Na	0.31	0.60	0.61	0.47	0.00	1.25	0.30	0.75	0.83	0.73	0.55	0.11	0.53	0.02	0.59	0.61	0.42	0.64	0.00	0.38	1.30	0.36	0.37
K	0.25	0.24	0.28	0.28	0.26	0.17	0.25	0.30	0.29	0.25	0.24	0.30	0.32	0.31	0.27	0.27	0.29	0.20	0.57	0.27	0.25	0.28	0.27
Total	15.3	15.4	15.7	15.5	15.2	15.4	15.3	15.8	15.9	15.6	15.4	15.4	15.7	15.4	15.7	15.6	15.6	15.4	16.5	15.3	15.4	15.4	15.3
$Mg/(Mg+Fe^{+2})$	0.46	0.75	0.50	0.50	0.31	1.00	0.47	0.53	0.52	0.58	0.57	0.34	0.46	0.37	0.49	0.57	0.41	0.50	0.13	0.52	0.45	0.47	0.48
Mg# (Mg-number)=Mg / ($Mg+Fe^{+2}$).																							

Appendix Table 3 . (Continued).

Amphibole, cont. (P11)

Tracydacite-Amphibole																			
Sample no	P11-1	P11-2	P11-3	P11-4	P11-5	P11-6	P11-7	P11-8	P11-9	P11-11	P11-12	P11-13	P11-14	P11-15	P11-16	P11-17	P11-18	P11-19	P11-20
SiO2	44.72	39.86	41.65	42.19	46.05	40.36	39.89	42.35	40.64	41.37	41.49	42.21	44.76	43.59	44.35	40.62	46.55	44.18	40.13
TiO2	1.95	2.19	1.36	1.97	2.41	1.78	1.42	1.68	1.64	1.33	2.07	2.11	1.69	1.51	1.77	130	1.49	2.75	1.85
Al2O3	14.58	13.42	14.05	13.18	11.62	14.64	15.50	15.94	14.59	14.42	15.26	14.30	14.50	14.68	13.84	15.83	14.90	15.80	14.57
FeO	18.33	12.50	15.87	18.94	18.91	16.13	17.04	18.30	16.54	17.34	17.82	17.71	18.49	17.34	16.51	16.05	19.07	18.50	17.13
MnO	0.50	0.01	0.00	0.53	0.22	0.15	0.06	0.40	0.14	0.41	0.44	0.27	0.21	0.00	0.00	0.03	0.48	0.10	0.20
MgO	8.68	8.89	8.55	7.75	5.39	11.14	10.28	9.18	9.63	11.26	9.10	8.35	7.79	9.74	8.12	11.02	9.11	8.02	8.77
CaO	10.94	11.92	9.70	11.67	11.93	10.27	9.73	10.19	10.92	10.06	10.70	11.,99	10.97	9.51	10.09	9.33	11.31	12.70	10.12
Na2O	0.87	1.61	1.06	0.37	0.00	2.76	2.49	1.51	2.02	2.65	1.42	0.81	0.62	1.65	1.36	3.25	0.94	0.50	1.58
K2O	0.90	0.94	1.02	1.35	1.02	0.96	0.95	0.93	0.97	0.81	1.00	1.16	1.02	0.80	1.10	0.97	1.18	1.28	0.93
On the basis of 32 oxygen																			
Si	6.32	6.31	6.35	6.30	6.89	5.88	5.84	6.00	6.05	5.91	6.00	6.23	6.44	6.22	6.56	5.86	6.36	6.22	6.05
Al^{IV}	1.68	1.69	1.65	1.70	1.11	2.12	2.16	2.,00	1.95	2.09	2.00	1.77	1.56	1.78	1.44	2.14	1.64	1.78	1.95
Al^{VI}	0.74	0.81	0.88	0.62	0.94	0.40	0.51	0.66	0.61	0.34	0.60	0.71	0.90	0.69	0.97	0.55	0.76	0.84	0.64
Fe^{+3}	0.82	0.00	0.78	0.54	0.00	1.16	1.41	1.30	0.73	1.51	1.05	0.35	0.55	1.25	0.28	1.34	0.81	0.17	0.99
Ti	0.21	0.26	0.16	0.22	0.27	0.20	0.16	0.18	0.18	0.14	0.23	0.23	0.18	0.16	0.20	0.14	0.15	0.29	0.21
Cr	0.00	0.00	0.00	0.00	0.00	0.00	0.00	0.00	0.00	0.00	0.00	0.00	0.00	0.00	0.00	0.00	0.00	0.00	0.00
Fe^{+2}	1.34	1.65	1.25	1.83	2.37	0.80	0.68	0.87	1.33	0.57	1.11	1.83	1.67	0.82	1.76	0.60	1.37	2.01	1.17
Mn	0.06	0.00	0.00	0.07	0.03	0.02	0.01	0.05	0.02	0.05	0.05	0.03	0.03	0.00	0.00	0.00	0.06	0.01	0.03
Mg	1.83	2.10	1.94	1.72	1.20	2.42	2.24	1.94	2.14	2.40	1.96	1.84	1.67	2.07	1.79	2.37	1.86	1.68	1.97
Ca	1.66	2.02	1.58	1.87	1.91	1.60	1.53	1.5	1.74	1.54	1.66	1.89	1.69	1.45	1.60	1.44	1.66	1.92	1.63
Na	0.24	0.49	0.31	0.11	0.00	0.78	0.71	0.,42	0.58	0.73	0.40	0.23	0.17	0.46	0.39	0.91	0.25	0.14	0.46
K	0.16	0.19	0.20	0.26	0.20	0.18	0.18	0.7	0.18	0.15	0.18	0.22	0.19	0.,15	0.21	0.18	0.21	0.23	0.18
Total	15.05	15.52	15.10	15.23	14.91	15.56	15.41	15.,13	15.51	15.42	15.24	15.35	15.05	15.06	15.19	15.53	15.11	15.28	15.27
Mg/(Mg+Fe2+)	0.58	0.56	0.61	0.49	0.34	0.75	0.77	0.69	0.62	0.81	0.64	0.50	0.50	0.72	0.50	0.80	0.58	0.46	0.63